

# Evolutionary synthesis of stellar populations: a modular tool

Claudia Maraston

*Department of Astronomy, University of Bologna, via Zamboni 33, 40126 Bologna, Italy*

Accepted Received ; in original form

## ABSTRACT

A new tool for the Evolutionary Synthesis of Stellar Populations (EPS) is presented, which is based on three independent matrices, giving respectively: 1) the fuel consumption during each evolutionary phase as a function of stellar mass; 2) the typical temperatures and gravities during such phases; 3) colours and bolometric corrections as functions of gravity and temperature. The modular structure of the code allows to easily assess the impact on the synthetic spectral energy distribution of the various assumptions and model ingredients, such as, for example, uncertainties in stellar evolutionary models, mixing length, the temperature distribution of horizontal branch (HB) stars, AGB mass loss, and colour-temperature transformations. The so-called “AGB-Phase Transition” in Magellanic Cloud clusters is used to calibrate the contribution of the Thermally Pulsing Asymptotic Giant Branch phase (TP-AGB) to the synthetic integrated luminosity. As an illustrative example, solar metallicity ( $Y = 0.27$ ,  $Z = 0.02$ ) models, with ages ranging between 30 Myr and 15 Gyr and various choices for the slope of the Initial Mass Function (IMF), are presented. Synthetic broad band colours and the luminosity contributions of the various evolutionary stages are compared with LMC and Galactic globular cluster data. In all these cases, a good agreement is found. Finally, we show the evolution of stellar mass-to-light ratios in the bolometric and  $U, B, V, R$ , and  $K$  passbands, in which the contribution of stellar remnants is accounted for.

**Key words:** galaxies: star clusters: evolution - galaxies: Magellanic Clouds - stars: AGB

## 1 INTRODUCTION

In order to study the formation and the subsequent evolution of galaxies, we have to understand the overall properties of their stellar content. In a galaxy, a mixture of stellar populations of different ages and chemical compositions are present and many efforts have been made in recent years, inspired by the pioneer work of Tinsley (1980), aimed at modelling the spectral evolution of the various morphological types, from ellipticals to spirals (e.g. Bruzual 1983; Arimoto & Yoshii 1987; Guiderdoni & Rocca-Volmerange 1987; Bruzual & Charlot 1993; Bressan, Chiosi & Fagotto 1994; Tantalo et al. 1996).

The building blocks of Evolutionary Population Synthesis (EPS) are models for Simple Stellar Populations (SSPs), that are assemblies of chemically homogeneous and coeval single stars. Thus, before facing the problem of modelling a complex stellar population, as a galaxy, the preliminary condition is to check the accuracy of SSPs computations and their adequacy to reproduce the observable features of stellar clusters, that better resembling the definition of SSP.

Two main approaches have been followed in computing EPS for SSPs. The ‘Isochrone Synthesis’ technique (Charlot & Bruzual 1991) consists in summing up the contributions to the flux in the various passbands of all mass-bins along one isochrone, after assuming an Initial Mass Function (IMF). The integration starts from a lower mass limit and ends at the latest mass point on the isochrone itself, that usually coincides with the end of the so-called Early Asymptotic Giant Branch (E-AGB) phase. Later stellar phases are then added following individual recipes (e.g. Charlot & Bruzual 1991). An alternative approach to compute the luminosity contributions of Post-Main Sequence evolutionary stages is based on the so-called Fuel Consumption theorem (FCT, Renzini & Buzzoni 1986). Here the main ingredient of synthesis is the amount of nuclear fuel (i.e. the hydrogen and/or helium mass) that is burned in each evolutionary stage. The fuel, a natural product of evolutionary stellar sequences, is converted into bolometric luminosity thanks to the FCT. The luminosities in the various passbands are then computed thanks to a temperature/gravity-colour set of transformations. In principle the two approaches are equivalent, as both

arXiv:astro-ph/9807338v1 31 Jul 1998

are based on stellar evolutionary models, but their practical implementations may result in sizable differences. In the isochrone synthesis method, the integration variable is the stellar mass, that varies along the isochrone. So, bright, but short-lived evolutionary stages span a very narrow range in stellar mass and integrations must use very small  $\Delta M$  steps. (We have noticed that mass steps as small as  $10^{-5} M_{\odot}$  are required to achieve a few per cent stability in numerical results.) Coarse mass zoning and poor interpolation algorithms are responsible for the sizable fluctuations occasionally exhibited by population models constructed with the isochrone synthesis method (see e.g. Fig. 7 in Charlot & Bruzual 1991). The method based on the FCT is instead much more robust in this respect, as the integration variable, the fuel, is directly proportional to the contribution of the various phases to the total luminosity.

At present this method has been followed by Buzzoni (1989) to construct SSPs for ages older than 4 Gyr. In this work we extend the approach to young and intermediate age populations and present SSP models for solar metallicity and ages from 30 Myr to 15 Gyr. The synthesis computational code has been constructed with the aim of better controlling the influence of various model ingredients on SSP models. The comparison with Magellanic Clouds and Galactic globular clusters allows a detailed test for the results. The paper is organised as follows. In Section 2 a detailed description of the algorithm is presented; Section 3 illustrates all model ingredients: stellar input and temperature-colour transformations. Section 4 describes the results and Section 5 shows the various observational tests performed. Finally, in Section 6, our conclusions are drawn.

## 2 THE ALGORITHM

The EPS code used in this paper is based on three independent sets of matrices containing the ingredients of the synthesis, namely:

- (i) *The energetics*: the nuclear fuel burned during each evolutionary phase as a function of stellar mass;
- (ii) *The surface parameters*: i.e. the effective temperatures and surface gravities during such phases;
- (iii) *The transformations to observables*: i.e. colours and bolometric corrections as functions of gravity and temperature.

Following Renzini & Buzzoni (1986; hereafter RB86), the total bolometric luminosity of a Simple Stellar Population (SSP) of age  $t$  can be written as the sum of two terms, one for the core hydrogen burning stars (the Main Sequence (MS) stars), one for the evolved ones (the Post-Main Sequence (PMS) stars)

$$L_T^{\text{bol}}(t) = L_{\text{MS}}^{\text{bol}}(t) + L_{\text{PMS}}^{\text{bol}}(t). \quad (1)$$

$L_{\text{MS}}^{\text{bol}}$  depends on the adopted mass-luminosity relation  $L(M, t)$  and Initial Mass Function (IMF)  $\Psi(M) = AM^{-(1+x)}$  ( $A$  being the scale factor giving the size of the stellar population).  $L_{\text{PMS}}^{\text{bol}}$  is directly connected with the total nuclear fuel burned by stars populating the various evolved stages, through the FCT (see 2.1).

To evaluate the MS bolometric luminosity, we need a set of isochrones, on which to perform a numerical integration weighted on the IMF

$$L_{\text{MS}}^{\text{bol}}(t) = \int_{M_{\text{inf}}}^{M_{\text{TO}}(t)} L(M, t) \Psi(M) dM \quad (2)$$

The lower integration limit is the minimum mass igniting H in the core ( $M_{\text{inf}}$ ).  $M_{\text{TO}}(t)$  (the turnoff mass) is the mass in the verge of exhausting hydrogen in the core and leaving the MS. We chose as  $M_{\text{TO}}(t)$  the model with the maximum effective temperature along the isochrone as, by definition, the turnoff point is the bluest point on the Hertzsprung-Russel (H-R) diagram. The relation between the age and the corresponding turnoff mass is the *evolutionary clock* of a stellar population.

### 2.1 Post-Main Sequence contributions: the Fuel Consumption Theorem

The Fuel Consumption theorem (FCT) states that: *the contribution of stars in any given Post-MS stage to the integrated bolometric luminosity of a SSP is directly proportional to the amount of fuel burned during that stage* (RB86). Its analytical form is

$$L_j^{\text{bol}}(t) = 9.75 \times 10^{10} b(t) F_j(M_{\text{TO}}) \quad (L_{\odot}) \quad (3)$$

where  $L_j^{\text{bol}}(t)$  is the total bolometric luminosity of stars populating the PMS stage  $j$  at the age  $t$ .  $b(t)$ , the “*evolutionary flux*”, is the number of stars evolving off the Main Sequence per year.  $F_j(M_{\text{TO}})$  is the nuclear fuel (in  $M_{\odot}$ ) burned by stars with  $M=M_{\text{TO}}$  in their  $j$ -th evolutionary PMS phase.

The function  $b(t)$  is defined as

$$b(t) = \Psi(M_{\text{TO}}) \left| \frac{dM_{\text{TO}}}{dt} \right| \quad (\text{stars/yr}) \quad (4)$$

where  $\Psi(M_{\text{TO}})$  is the IMF computed for  $M = M_{\text{TO}}$  and  $\dot{M}_{\text{TO}}$  is the time derivative of the relation  $M_{\text{TO}}(t)$ . At any SSP age, the mass of evolved stars is only slightly greater than  $M_{\text{TO}}(t)$ . Hence, to a fair approximation  $b(t)$  also gives the rate at which stars enter or leave any specific post-MS evolutionary stage.

The fuel consumption  $F_j$  is given by

$$F_j = m_j^{\text{H}} + 0.1m_j^{\text{He}} \quad (M_{\odot}) \quad (5)$$

where  $m_j^{\text{H}}$  and  $m_j^{\text{He}}$  are the amount of hydrogen and helium burned during the phase  $j$ , the coefficient 0.1 taking into account that the energy release from helium-burning is  $\simeq 1/10$  than from H-burning. The close coincidence in mass between evolved stars and  $M_{\text{TO}}(t)$  allows us to refer the PMS fuels to the values proper to a mass equal to  $M_{\text{TO}}(t)$ . As a consequence, mass and age indices are equivalent for PMS stars and the index  $j$  will be used to label star masses in the MS and evolutionary stages in the PMS.

This approximation, in which one assumes the flux  $b(t)$  to be constant through the various PMS stages, was extensively criticized by Charlot & Bruzual 1991. However, it has been demonstrated that this is actually a very accurate approximation (Renzini 1994).

## 2.2 From Bolometric to Monochromatic

To compute the SSP total luminosity in the generic photometric band  $\lambda$ , i.e.

$$L_T^\lambda(t) = L_{MS}^\lambda(t) + L_{PMS}^\lambda(t), \quad (6)$$

we need temperature/gravity - bolometric correction/colour sets of transformations. The  $(T_e, g)_{ij}$  matrix contains the effective temperatures and the surface gravities of stars in the  $j$ -th phase, at the SSP age  $i$  (see 3.3 for a detailed description of adopted values). The colour index/bolometric correction matrix  $(CI, BC)_{lm}$  contains the transformations to the observables, i.e. bolometric corrections and colours as functions of the surface parameters  $(T_e, g)$ .  $l$  is an effective temperature index and  $m$  refers to surface gravity: we defer to 3.4 for a detailed description of adopted sets. The  $\lambda$ -luminosity of the  $j$ -star at the SSP age  $i$ ,  $L_{ij}^\lambda$ , is a fraction of its bolometric luminosity  $L_{ij}^{\text{bol}}$ , as

$$L_{ij}^\lambda = Q_{ij}^\lambda \cdot L_{ij}^{\text{bol}} \quad (L_{ij}^\lambda) \quad (7)$$

Luminosities in eq. (7) are in solar units and  $Q_{ij}^\lambda$  is defined as

$$Q_{ij}^\lambda = 10^{-0.4[BC_\odot^\lambda - BC_{ij}^\lambda]} \quad (8)$$

where  $BC_{ij}^\lambda$  is the bolometric correction to the  $\lambda$ -band and  $BC_\odot^\lambda$  the same for the Sun.

In order to get the luminosity contributions of PMS phases, we divide each phase  $j$  into a certain number of photometric sub-phases, burning an equal fraction of the total fuel  $F_{ij}$  and having a constant  $Q$ -factor (eq. 8). Then we apply eq. (7), summing over these sub-phases. The SSP total  $\lambda$ -luminosity at the age  $i$  is finally

$$L_{i,T}^\lambda = \sum_j L_{ij}^\lambda \quad (9)$$

A correct link between MS and PMS luminosity contributions is ensured by adopting the same normalization constant  $A$  for  $\Psi(M)$  in eq. (2) and (3).

The modular structure of the code allows to easily change a particular ingredient and/or assumption, independently of the others, as assessing just its own impact in the final output (see 5.4 for some examples).

## 3 MODEL INGREDIENTS

In this section we describe all adopted model ingredients. The stellar stages included in the synthesis range from the Main Sequence to the end of the Thermally Pulsing Asymptotic Giant Branch (TP-AGB). The Post-AGB has not been taken into account as the  $UV$  output of old populations is extremely model dependent (cf. Greggio & Renzini 1990).

### 3.1 Stellar input

For the MS mass-luminosity relation  $L(M, t)$  (eq. 2), a homogeneous set of solar chemical composition ( $Y = 0.27, Z = 0.02$ ) isochrones (Castellani, Chieffi & Straniero 1992, hereafter CCS92), with ages ranging from 30 Myr to 10 Gyr has been adopted. An additional isochrone for 15 Gyr has been constructed from the same set of stellar tracks kindly provided by Oscar Straniero. The dwarf-MS component down

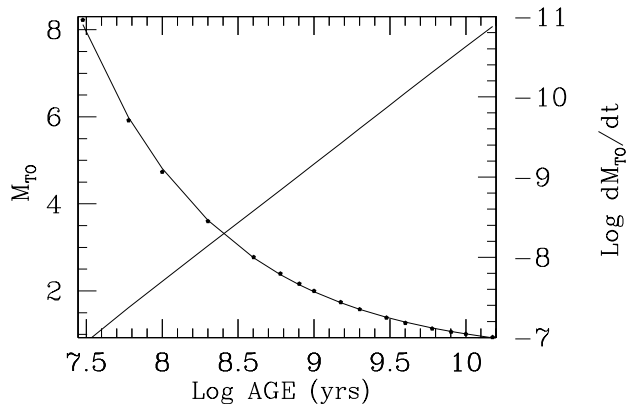


**Figure 1.** The relation  $M_{\text{TO}}(t)$  and its time derivative  $\dot{M}_{\text{TO}}(t)$  (in yr,  $M_{\text{TO}}$  in  $M_\odot$ ). The relation has been obtained via an analytical fit on CCS92 isochrones.

to  $0.1 M_\odot$ , has been added using the models of Vandenberg et al. (1983) for  $Y=0.25, Z=0.02$ . The small difference in the helium content is not crucial in this context, as the location of the lower Main-Sequence, in the  $\log L - \log T_e$  plane, strongly depends on metallicity, but it is rather insensitive to the small variations of  $Y$  parameter.

The relation  $M_{\text{TO}}/\text{age}$  (Fig. 1) is obtained via an analytical fit on CCS92 isochrones

$$\log M_{\text{TO}}(t) = a \log t + b \log^2 t + c \log^3 t + d \quad (10)$$

where  $a = 0.212567$ ,  $b = -0.108394$ ,  $c = 0.005737$ ,  $d = 2.981730$  ( $M_{\text{TO}}$  in  $M_\odot$ ,  $t$  in yr). The time derivative of  $M_{\text{TO}}(t)$  is also displayed in Fig. 1. As it is evident, the SSP evolutionary clock,  $\dot{M}_{\text{TO}}$ , is very fast for the large values of  $M_{\text{TO}}$ , then its rate drops greatly as  $M_{\text{TO}}$  decreases. In fact,  $M_{\text{TO}}$  ranges from  $\simeq 8.3$  at  $t = 30$  Myr to  $\simeq 0.94$  at  $t = 15$  Gyr while, in the same age range,  $\dot{M}_{\text{TO}}$  drops by more than 4 orders of magnitude. This implies a faster SSP luminosity evolution at young ages ( $t \lesssim 1$  Gyr).

The stellar evolutionary tracks used to derive eq. (10) have been constructed using canonical assumptions concerning convective boundaries, i.e. no overshooting. Slightly higher values of  $M_{\text{TO}}$  for given age are obtained when allowing for convective overshooting, the size of the effect depending on a free parameter. However, no general agreement has yet emerged as to what value should be assigned to the free parameter, and therefore we prefer to use canonical models.

Fig. 2 shows the evolutionary flux  $b(t)$ , i.e. the rate of evolution off the Main Sequence (eq. 4), for four different choices of the IMF slope. The functions  $b(t)$  are normalized at  $b = 1$  for  $t = 15$  Gyr, thus a comparison between the different slopes is possible regardless of the SSP size.  $b(t)$  is the product of two terms: one increasing ( $\Psi$ ) and one decreasing ( $\dot{M}_{\text{TO}}$ ) with age. The flatter the IMF, the slower the increase

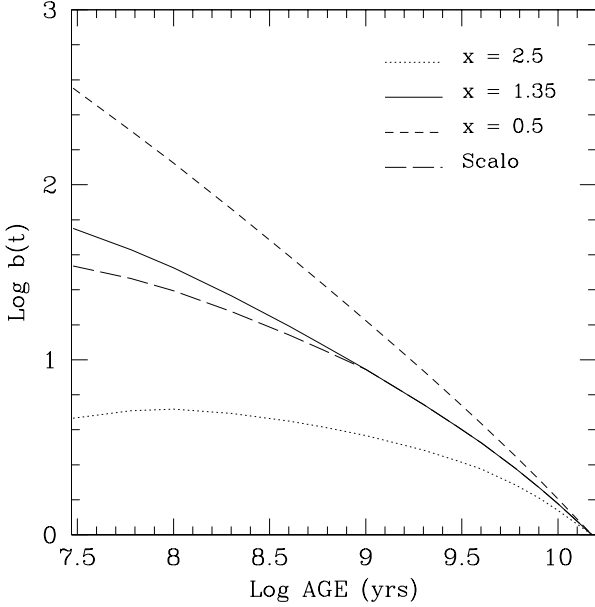


**Figure 2.** The evolutionary flux  $b(t)$  for three choices of the IMF slope  $x$ . The effect of a multislope, like a Scalo type, is also shown, in which  $x$  is  $-1$  for  $M \leq 0.3$ ,  $1.35$  for  $0.3 < M \leq 2$ ,  $1.7$  otherwise. Functions  $b(t)$  are normalized at  $t = 15$  Gyr.

in time of  $\Psi(M)$  and the rapid decrease in  $\dot{M}_{\text{TO}}$  dominates. This results in a greater SSP luminosity evolution for flatter IMFs.

### 3.2 The Fuel Consumption matrix $F_{ij}$

Table 1 is our  $F_{ij}$  matrix. It gives the amount of hydrogen and helium (in  $M_{\odot}$ ) that are burned by a star of mass  $M_{\text{TO},i}$  in each of its PMS stages. The total nuclear fuel follows from eq. (5), while  $M_{\text{TO},i}$  and the corresponding age are related by eq. (10). The adopted values of  $F_{ij}$  in Table 1 are basically the same as those used by Renzini (1992). They have been derived from various sets of evolutionary sequences, including Sweigart & Gross (1978), Becker (1981), Sweigart, Greggio & Renzini (1989), Renzini & Voli (1981), and Greggio & Renzini (1990). These data have been complemented with data from Chieffi & Straniero (1992, *private communication*) for the fuel consumption during the RGB phase. In principle it would have been most appropriate to use fuel consumption data from a unique, homogeneous set of evolutionary calculations. Unfortunately, such a complete set, covering all evolutionary phases for all stellar masses is still not available. However, the present compromise is largely adequate for the scope of this paper.

A special care was devoted to estimate the fuel consumption during the TP-AGB phase. Uncertainties in mass loss, mixing, and efficiency of hydrogen burning at the bottom of the convective envelope (known as envelope burning process) together prevent pure theory from predicting the amount of fuel burned during this stage (RB86). The uncalibrated models of Renzini and Voli (1981, hereafter RV81) used by RB86 largely overestimate the TP-AGB contribution for populations younger than  $\sim 10^8$  yr in comparison with the observed contribution in Magellanic Cloud clusters

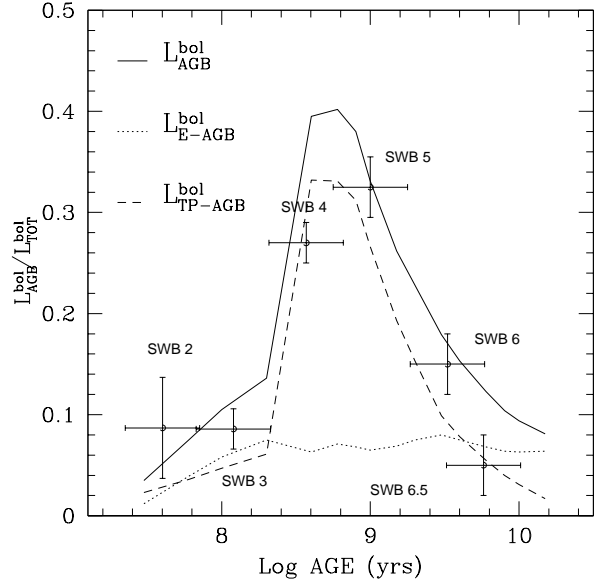


**Figure 3.** The synthetic AGB bolometric contribution compared with LMC GCs data from FMB90. E-AGB and TP-AGB contributions are also shown separately. Each data point has been obtained through a procedure aimed at minimizing the stochastic fluctuations between clusters having an equal SWB parameter (see the text). Error bars indicate the r.m.s.

in the corresponding age range (Frogel, Mould & Blanco 1990, hereafter FMB90).

The origin of the discrepancy has been controversial for several years, but a decisive hint came from the discovery that TP-AGB stars experiencing the envelope burning process do not follow the canonical AGB core mass-luminosity relation (Blöcker & Schönberner 1991). The  $7 M_{\odot}$  model by Blöcker & Schönberner is much more luminous and evolves  $\sim 10$  times faster than that predicted by the standard core mass-luminosity relation (e.g. Paczynski 1970a,b) that was used by RV81. The consequence is a drastic decrease of the TP-AGB lifetime and of the TP-AGB fuel consumption, that results in a lower contribution of this phase to the integrated light of a population.

The transition between TP-AGB stars that experience the envelope burning process and those which do not is very sharp, and takes place at a threshold mass that depends sensitively to the mixing length parameter  $\alpha$  (RV81). Now, Magellanic Cloud clusters offer an opportunity to calibrate this parameter in such a way to reproduce the observed contribution of AGB stars. Following Blöcker & Schönberner (1991) we assume that TP-AGB stars experiencing envelope burning consume  $\sim 10$  times less fuel than predicted by RV81, while we retain RV81 fuel consumptions for stars that do not experience envelope burning. In this way the calibration procedure reduces to find the value of  $\alpha$  that best accounts for the data. The result is shown in Fig. 3 which compares the theoretical AGB contributions for  $\alpha = 2$  to the Magellanic Cloud cluster data from FMB90. For this value of  $\alpha$  stars more massive than  $\sim 3 M_{\odot}$  experience the envelope burning process and have the TP-AGB fuel consumption correspondingly reduced.

**Table 1.** The  $F_{ij}$  matrix: the masses of hydrogen ( $m_{\text{H}}$ ) and helium ( $m_{\text{He}}$ ) (both in  $M_{\odot}$ ) burned in each evolutionary PMS  $j$  phase, namely SGB, RGB, HB, E-AGB, TP-AGB, by a star of  $M = M_{\text{TO},i}$  ( $i$  is the age index). Values are the same as in Renzini (1992; see the text).

AGE (Gyr)	$M_{\text{TO},i}$	SGB	RGB	HB		E-AGB		TP-AGB	
		$m_{\text{H}}$	$m_{\text{H}}$	$m_{\text{H}}$	$m_{\text{He}}$	$m_{\text{H}}$	$m_{\text{He}}$	$m_{\text{H}}$	$m_{\text{He}}$
0.03	8.2247	0.0222	0.0058	0.3116	0.8280	0.0000	0.2091	0.0339	0.0491
0.06	5.9188	0.0267	0.0059	0.1898	0.5211	0.0000	0.4210	0.0339	0.0491
0.1	4.7334	0.0296	0.0046	0.1482	0.3993	0.0015	0.4567	0.0339	0.0491
0.2	3.6001	0.0323	0.0031	0.1233	0.3115	0.0081	0.3918	0.0339	0.0491
0.4	2.7777	0.0331	0.0041	0.1109	0.2647	0.0110	0.3448	0.2071	0.3138
0.6	2.3977	0.0329	0.0108	0.1136	0.2366	0.0181	0.2971	0.1931	0.2927
0.8	2.1640	0.0315	0.0388	0.1108	0.2201	0.0153	0.2867	0.1744	0.2643
1	1.9985	0.0307	0.0993	0.0815	0.2349	0.0119	0.2802	0.1427	0.2163
1.5	1.7408	0.0364	0.1453	0.0668	0.2386	0.0107	0.2969	0.0979	0.1483
2	1.5784	0.0431	0.1595	0.0621	0.2373	0.0113	0.3083	0.0747	0.1132
3	1.3844	0.0509	0.1689	0.0646	0.2472	0.0139	0.2921	0.0463	0.0701
4	1.2651	0.0572	0.1806	0.0618	0.2594	0.0116	0.2827	0.0363	0.0550
6	1.1341	0.0625	0.1885	0.0595	0.2665	0.0090	0.2750	0.0254	0.0384
8	1.0588	0.0653	0.1921	0.0583	0.2693	0.0076	0.2710	0.0191	0.0289
10	1.0110	0.0660	0.1947	0.0560	0.2671	0.0086	0.2671	0.0151	0.0228
15	0.9380	0.0659	0.1991	0.0508	0.2598	0.0124	0.2598	0.0090	0.0136

In Magellanic Cloud clusters the number and luminosity of AGB stars is subject to large fluctuations from one cluster to another of similar age, and therefore so does the AGB contribution to the total light. This is a result of small number statistics, as clusters contain at most just a few AGB stars. To cope with this problem, clusters have been grouped in age bins following the classification of Searle, Wilkinson and Bagnuolo (1980), with the SWB type being related to age by the relation given by FMB90. Within each bin the AGB contribution to the bolometric luminosity was then obtained by adding together the luminosity of all the AGB stars in the binned clusters, and dividing by the sum of all the integrated luminosities of the same clusters. Fig. 3 shows that a jump in the AGB contribution takes place between SWB type III and SWB type V, or at an age of  $\sim 0.2$  Gyr, with the AGB contribution suddenly increasing from  $\sim 10$  per cent to over  $\sim 30$  per cent. This corresponds to the so-called ‘‘AGB phase transition’’ (RB86) due to the development of a bright and well populated TP-AGB phase (see also Renzini 1992).

The TP-AGB phase is populated by C and M spectral type stars. The production of C (carbon) stars is a function of both metallicity and the initial stellar mass, hence of the SSP age (cf. RV81). From FMB90 data for LMC clusters (their Table 4) we have evaluated the C and M star luminosity contributions to the total light for each age bin. As  $L_{\text{TP-AGB}}^{\text{bol}} \propto F_{\text{TP-AGB}}$  (eq. 3), we have then calibrated the fractions of TP-AGB fuel burned by M and C stars as functions of SSP age. The use of LMC GCs as calibrators is unavoidable, as they represents the only available sample of clusters covering a broad age-range and being populous enough, so ensuring that the AGB is reasonably well sampled. These clusters have typically  $\sim 1/2 Z_{\odot}$  metallicity, but a similar sample for solar metallicity is not available. The dependence on  $Z$  may be taken into account using the prescriptions of RV81. This will be discussed in sec. 5.4.2.

The calibration is shown in Table 2 (and Fig. 4). As it can be noticed, carbon stars characterize intermediate age

**Table 2.** The calibration of the TP-AGB fuel (see the text). Column 2 give the total TP-AGB fuel, Column 3 and 4 its fraction burned by C and M type stars respectively, as functions of the SSP age.

AGE(Gyr)	$F_{\text{TP-AGB}}$	$\%F_{\text{TP-AGB}}^{\text{C}}$	$\%F_{\text{TP-AGB}}^{\text{M}}$
0.03	0.0388	0.0000	1.0000
0.06	0.0388	0.0000	1.0000
0.1	0.0388	0.0000	1.0000
0.2	0.0388	0.0000	1.0000
0.4	0.2385	0.1138	0.8862
0.6	0.2224	0.1138	0.8917
0.8	0.2008	0.1160	0.9019
1	0.1643	0.1421	0.8579
1.5	0.1127	0.1065	0.8935
2	0.0860	0.0846	0.9154
3	0.0533	0.0689	0.9311
4	0.0418	0.0583	0.9417
6	0.0292	0.0657	0.9343
8	0.0220	0.0000	1.0000
10	0.0174	0.0000	1.0000
15	0.0104	0.0000	1.0000

SSPs, those having a developed TP-AGB. Very old stellar populations (e.g. galactic globular clusters and the Galactic Bulge) do not have C stars, in agreement with theoretical expectations.

Fig. 5 shows the total amount of fuel burned in the whole PMS,  $F_{i,T} = \sum_j F_{ij}$ , as a function of the SSP age and the turnoff mass. The total fuel decreases with the decreasing mass, till the onset of AGB phase transition, at ages around 0.2 Gyr. Starting from  $t \gtrsim 1$  Gyr,  $F_{i,T}$  tends to remain nearly constant as the decrease in the TP-AGB fuel is partly compensated by the increase in the fuel burned on the red giant branch (RGB). This epoch is referred to as ‘‘RGB phase transition’’ (RB86), the mass at the transition being around  $\simeq 2.5 M_{\odot}$ , in dependence of the chemical composi-

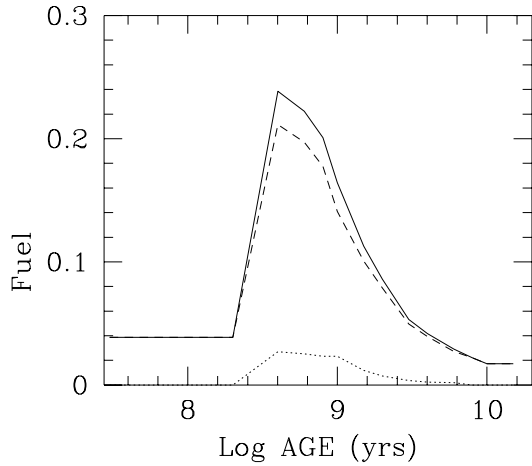


**Figure 4.** The total amount of TP-AGB fuel (*solid line*), its fraction burned by C type stars (*dotted line*) and by M type stars (*dashed line*), as functions of age (see the text).

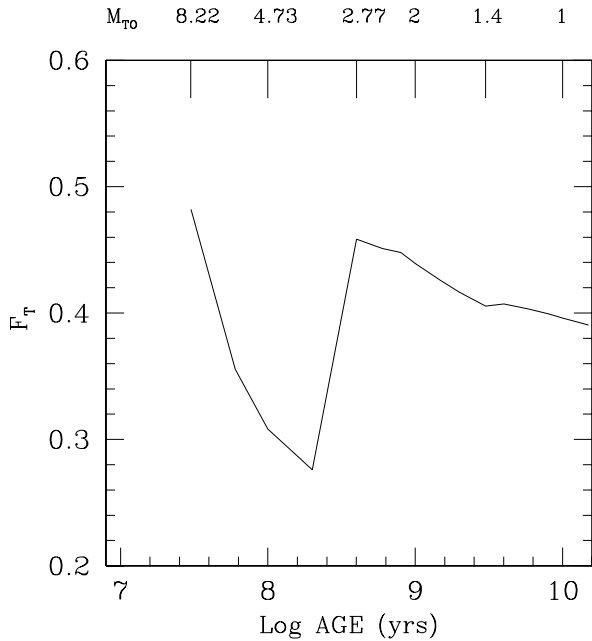


**Figure 5.** The total fuel consumption (in  $M_{\odot}$ ) during the whole post-MS, as a function of the SSP age (*lower scale*) and the corresponding turnoff mass (*upper scale*).

tion. As it can be noticed, the PMS total fuel depends only weakly on age, ranging from  $\simeq 0.5 M_{\odot}$  at  $t \simeq 30$  Myr to  $\simeq 0.4 M_{\odot}$  at  $t \simeq 15$  Gyr. Also, it is possible to show that the MS luminosity contribution tends to be nearly constant after an age of  $\simeq 1$  Gyr. As a consequence, the luminosity evolution of a SSP is mainly controlled by the evolutionary flux  $b(t)$ . Fig. 6 shows the time evolution of the fuel consumptions in the various phases. Worth noting is the sharp

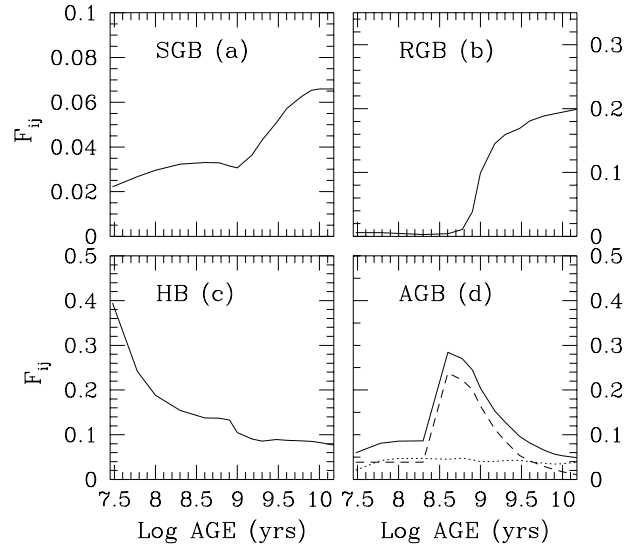


**Figure 6.** The fuel consumption in each evolutionary PMS phase  $j$  as function of the SSP age; in panel (d),  $F_{E-AGB}$  (*dotted line*) and  $F_{TP-AGB}$  (*dashed line*) are separately shown.

increase of the RGB fuel consumption at  $t \simeq 1$  Gyr, which is due to the appearance of stars developing a degenerate helium core, a phenomenon known as RGB phase transition (RB86, Sweigart, Greggio & Renzini 1990). The small hump in the HB fuel consumption at nearly this same age is also due to the RGB phase transition, with stars with a minimum value of the core mass populating the HB, hence experiencing a prolonged HB phase leading to a local maximum in the hydrogen consumption (cf. Table 1).

Finally, Fig. 7 shows the contribution of various evolutionary stages to the total bolometric luminosity,  $L_{ij}^{\text{bol}}/L_{i,T}^{\text{bol}}$ , obtained with the procedure described in sec. 2 and the ingredients of sec. 3.1 and 3.2. The energetic of young SSPs ( $t \lesssim 0.3$  Gyr) is dominated by MS stars, that of intermediate age ones ( $0.3 \lesssim t \lesssim 3$  Gyr) by AGB stars and, finally, by RGB stars for  $t \gtrsim 3$  Gyr. For ages older than  $\simeq 6$  Gyr, the relative MS contribution tends to rise. This effect is caused by the MS integrated luminosity decreasing slower than  $b(t)$ . As the total fuel keeps nearly constant, the net result is a lower total luminosity as mainly due to a lower PMS luminosity.

### 3.3 The temperature/gravity matrix $(T_e, g)_{ij}$

The  $(T_e, g)_{ij}$  matrix contains the distribution of effective temperatures and surface gravities of the evolutionary phases  $j$  at the SSP age  $i$ .

Stellar effective temperatures depend crucially on the efficiency of convective energy transfer, parametrized by the mixing length parameter  $\alpha$ . The use of uncalibrated theoretical effective temperatures in EPS computations is extremely dangerous, as the calibration of  $\alpha$  is the synchronization of the EPS clock. CCS92 isochrones are computed for  $\alpha = 1.6$ , a value that matches the observed Sun. Moreover, these isochrones have been tested on a sample of well-studied

**Table 3.** The  $(T_e, g)_{ij}$  matrix for the 30 Myr, the 1 Gyr and the 15 Gyr SSP: effective temperatures and surface gravities for the  $j$  evolutionary phases, as functions of the  $i$  ages. Values have been drawn from CCS92 isochrones.

MS		SGB		RGB		HB		E-AGB	
$\log g$	$\log T_e$	$\log g$	$\log T_e$	$\log g$	$\log T_e$	$\log g$	$\log T_e$	$\log g$	$\log T_e$
AGE = 30 Myr									
4.76	3.6044	3.77	4.3148	1.42	3.6537	0.88	3.6092	0.89	3.6154
4.59	3.7128	3.76	4.3120	1.32	3.6397	0.95	3.6206	0.70	3.5998
4.38	3.8055	3.75	4.3095	1.14	3.6248	0.96	3.6235	0.75	3.6032
4.32	3.8880	3.74	4.3075	0.99	3.6144	1.03	3.6554	0.65	3.5956
4.33	3.9614	3.73	4.3059	0.93	3.6100	1.64	3.8188	0.56	3.5890
4.33	4.0165	3.63	4.2824	0.90	3.6082	1.75	3.8491	0.48	3.5838
4.31	4.0585	3.53	4.2636	0.89	3.6071	1.83	3.8723	0.42	3.5794
4.29	4.0949	3.45	4.2457	0.87	3.6064	1.90	3.8925	0.35	3.5749
4.27	4.1269	3.37	4.2259	0.87	3.6058	1.96	3.9114	0.28	3.5704
4.25	4.1545	3.27	4.2020	0.86	3.6052	1.98	3.9191	0.20	3.5650
4.23	4.1781	3.15	4.1709	0.85	3.6046	2.02	3.9315		
4.20	4.1991	2.99	4.1274	0.84	3.6040	2.07	3.9473		
4.17	4.2178	2.76	4.0594	0.84	3.6036	2.06	3.9451		
4.14	4.2338	2.33	3.9343	0.83	3.6033	2.05	3.9419		
4.10	4.2480			0.83	3.6031	2.04	3.9383		
4.06	4.2602			0.83	3.6029	2.02	3.9343		
4.01	4.2701			0.82	3.6028	1.99	3.9273		
3.95	4.2771			0.82	3.6027	1.94	3.9156		
3.88	4.2800			0.82	3.6026	1.88	3.8980		
3.78	4.2776			0.82	3.6025	1.77	3.8704		
3.67	4.2725			0.82	3.6024	1.60	3.8225		
3.67	4.2767			0.82	3.6024	1.12	3.6905		
3.77	4.3161			0.82	3.6023				
AGE = 1 Gyr									
4.76	3.6044	3.85	1.4166	3.42	3.7177	2.71	3.6860	2.45	3.6764
4.71	3.6194	3.83	3.8927	3.34	3.7086	2.71	3.6876	2.10	3.6562
4.66	3.6416	3.82	3.8901	3.25	3.7031	2.71	3.6881	2.19	3.6617
4.62	3.6706	3.80	3.8872	3.16	3.6990	2.72	3.6885	2.19	3.6618
4.60	3.6990	3.78	3.8842	3.08	3.6957	2.72	3.6888	2.18	3.6614
4.56	3.7240	3.76	3.8801	3.00	3.6925	2.72	3.6891	2.16	3.6604
4.52	3.7455	3.74	3.8759	2.93	3.6897	2.72	3.6894	2.13	3.6584
4.47	3.7618	3.71	3.8692	2.86	3.6867	2.72	3.6897	2.08	3.6553
4.42	3.7770	3.67	3.8604	2.79	3.6842	2.72	3.6899	1.98	3.6498
4.37	3.7914	3.63	3.8475	2.73	3.6813	2.72	3.6901	1.81	3.6401
4.34	3.8066	3.56	3.8284	2.67	3.6788	2.72	3.6903	1.32	3.6099
4.30	3.8201	3.48	3.8029	2.60	3.6758	2.71	3.6905		
4.26	3.8318	3.42	3.7735	2.55	3.6758	2.71	3.6908		
4.22	3.8415	3.42	3.7425	2.49	3.6708	2.70	3.6910		
4.19	3.8525			2.44	3.6708	2.69	3.6909		
4.16	3.8619			2.40	3.6666	2.68	3.6907		
4.12	3.8687			2.35	3.6641	2.67	3.6901		
4.08	3.8727			2.31	3.6626	2.65	3.6893		
4.01	3.8726			2.11	3.6516	2.62	3.6872		
3.93	3.8666			1.98	3.6451				
3.83	3.8571			1.64	3.6260				
3.83	3.8607			1.37	3.6103				
3.91	3.9057			0.97	3.5858				

Galactic clusters and account well for the observed location of stars in the various evolutionary stages (see CCS92). The  $(T_e, g)_{ij}$  values for MS to E-AGB have been taken from CCS92 calibrated isochrones. V83 models have been used for the dwarf-Main Sequence component ( $0.1 \leq M < 0.6$ ).

For the TP-AGB phase, the relative proportions of C and M stars as functions of age (from FMB90, see sec. 3.2)

are used as indicators of the evolution of the spectral type along the TP-AGB.

The time evolution of the  $T_e$  ranges spanned by PMS evolutionary stages is displayed in Fig. 8, while Fig. 9 shows the same for the MS. To note in Fig. 8 the red HB clump at late ages (see 5.4.1). As an example, Table 3 is the  $(T_e, g)_{ij}$  matrix for  $i=30$  Myr, 1 Gyr and 15 Gyr ( $M_{TO} = 8.2247$ ,

**Table 3** – *continued*

MS		SGB		RGB		HB		E-AGB	
$\log g$	$\log T_e$	$\log g$	$\log T_e$	$\log g$	$\log T_e$	$\log g$	$\log T_e$	$\log g$	$\log T_e$
AGE = 15 Gyr									
4.74	3.6065	4.29	3.7455	3.93	3.7102	2.26	3.6607	2.02	3.6486
4.70	3.6175	4.23	3.7458	3.84	3.6961	2.29	3.6621	1.53	3.6183
4.66	3.6298	4.24	3.7461	3.81	3.6938	2.28	3.6630	1.69	3.6294
4.68	3.6539	4.22	3.7464	3.79	3.6920	2.30	3.6640	1.71	3.6305
4.66	3.6632	4.18	3.7456	3.76	3.6901	2.31	3.6649	1.71	3.6302
4.65	3.6681	4.17	3.7445	3.73	3.6888	2.31	3.6657	1.70	3.6298
4.64	3.6732	4.15	3.7429	3.69	3.6876	2.31	3.6665	1.68	3.6283
4.63	3.6783	4.13	3.7407	3.66	3.6864	2.34	3.6670	1.62	3.6261
4.62	3.6835	4.09	3.7379	3.63	3.6858	2.32	3.6674	1.60	3.6231
4.61	3.6887	4.07	3.7344	3.59	3.6850	2.32	3.6679	1.52	3.6191
4.59	3.6993	4.02	3.7298	3.55	3.6843	2.31	3.6680	1.46	3.6142
4.58	3.7040	3.99	3.7223	3.51	3.6836	2.31	3.6677		
4.57	3.7091			3.47	3.6829	2.31	3.6676		
4.56	3.7136			3.42	3.6819	2.30	3.6674		
4.54	3.7179			3.37	3.6811	2.29	3.6673		
4.53	3.7222			3.32	3.6802	2.28	3.6668		
4.51	3.7263			3.26	3.6794	2.27	3.6661		
4.49	3.7303			3.17	3.6774	2.26	3.6652		
4.47	3.7340			3.12	3.6761	2.23	3.6636		
4.45	3.7375			3.03	3.6742	2.18	3.6596		
4.43	3.7405			2.90	3.6712				
4.40	3.7436			2.77	3.6674				
4.39	3.7445			2.63	3.6616				
4.38	3.7450			2.56	3.6597				
4.35	3.7469			2.32	3.6504				
4.32	3.7479			1.86	3.6283				
4.27	3.7484			0.02	3.5179				

**Table 4.** The adopted solar normalization

$BC_{V\odot}$	$M_{bol\odot}$	$M_{U\odot}$	$M_{B\odot}$	$M_{V\odot}$	$M_{R\odot}$	$M_{K\odot}$
-0.08	4.75	5.61	5.48	4.83	4.31	3.41

1.9985 and 0.9380 respectively). By changing the content of the  $(T_e, g)$  matrix, it is possible to infer the impact on the integrated photometric features of SSPs, of some model parameters such as mixing length and mass loss, that directly influence effective temperatures and surface gravities (see 5.4).

### 3.4 The colour/bolometric correction matrix

The  $(CI, BC)_{lm}$  matrix contains bolometric corrections and colour indices, to distribute the total energy through the various passbands. It covers the range of  $(T_e, g)_{ij}$  matrix and contains empirical colours suitable to TP-AGB M and C type stars.  $BC_V$  and  $(U - B)$  are taken from Kurucz (1992) theoretical grids, on which a quadratical interpolation in  $\log T_e$ ,  $\log g$  has been performed. For  $T_e \leq 3500$  °K, the limit of Kurucz models, some extrapolations have been necessary.  $(B - V)$  colours have been taken from CCS92 isochrones. They are computed on the basis of the empirical color-temperature relation obtained by Arribas & Martinez (1988, 1989), for  $4000 K \leq T_e \leq 8000 K$  (see the authors for more details); outside this  $T_e$  range, they are based on Kurucz models.  $(V - R)$  and  $(V - K)$  colours, for spectral types earlier than K, have been taken from Johnson

(1966) empirical tables, on which a linear interpolation in  $(B - V)$  has been performed. For M type stars, the theoretical models by Bessel et al. (1989) have been used. Colours have been linearly interpolated in  $T_e$ . For M and C type TP-AGB stars  $(V - R)$  and  $(V - K)$  values have been taken from various sets of observational data (Cohen et al. 1981; Cohen 1982; Westerlund et al. 1991). Finally, Table 4 shows the adopted values for the solar normalization (from Allen 1991). By changing the  $(CI, BC)_{lm}$  matrix, it is possible to explore the influence on model output of the photometric ingredients and the associated uncertainties.

## 4 RESULTS

Evolutionary synthesis models for SSPs have been computed with the algorithm presented in Section 2 and the ingredients described in Section 3. Models are characterized by a solar chemical composition and ages ranging from 30 Myr to 15 Gyr. The model predicts the SSP photometric properties as functions of age, i.e. the broad-band colours  $(U - V)$ ,  $(U - B)$ ,  $(B - V)$ ,  $(V - R)$  and  $(V - K)$ , the bolometric corrections, the specific contributions of evolutionary phases to the bolometric and to the broad band luminosities, and the stellar mass-to-light ratios (see App. A, Tables A1, A2 for a complete list).



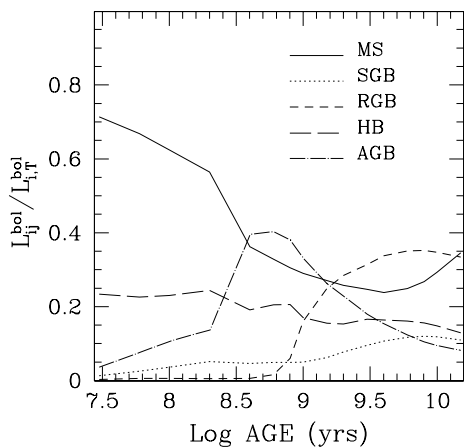


**Figure 7.** The time evolution of the relative contributions  $L_{ij}^{bol}/L_{i,T}^{bol}$  of stars in the various evolutionary stages to the integrated bolometric light of a stellar population.

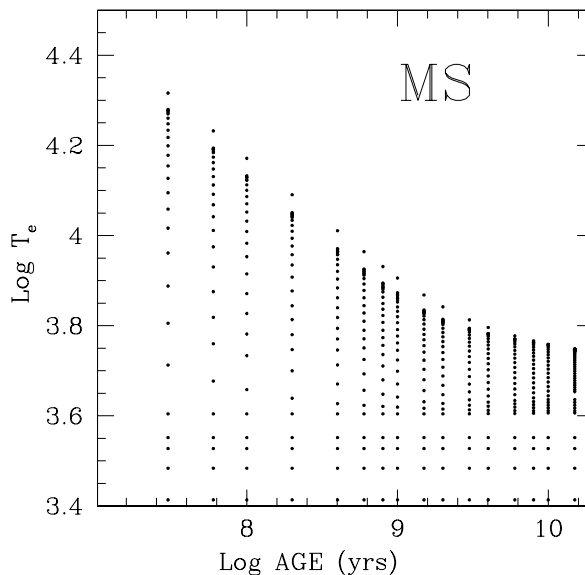


**Figure 9.** The same as Fig. 8 for the Main Sequence.

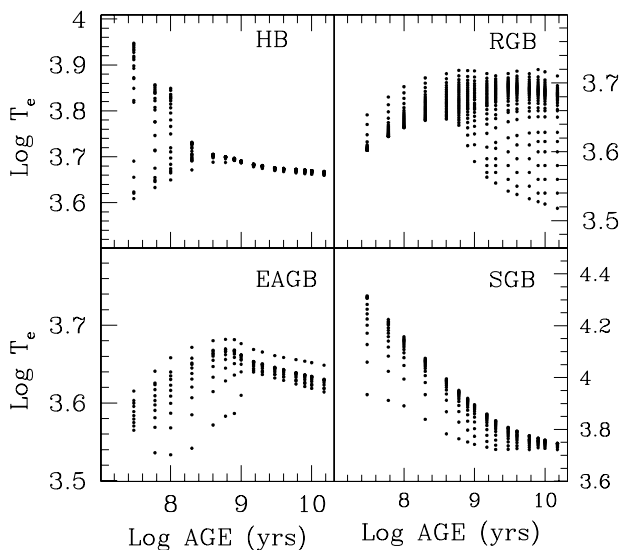


**Figure 8.** The time evolution of effective temperatures  $T_e$  in the evolutionary PMS stages.

#### 4.1 The time evolution of integrated colours

The time evolution of synthetic broad-band colours is shown in Fig. 10.

$(U-V)$ ,  $(U-B)$  and  $(B-V)$  colours vary smoothly with age, because they trace the turnoff effective temperature. The evolutionary trend of IR colours is instead controlled by the AGB and RGB phase transitions. Their impact is particularly evident in  $(V-K)$ , rising from  $\sim 1.3$  to  $\sim 3.2$

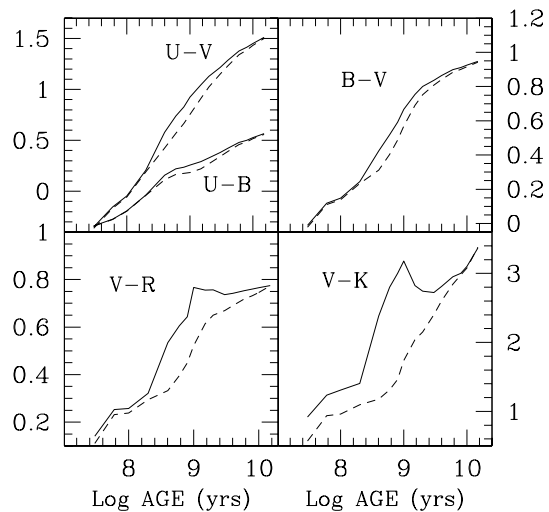


**Figure 10.** The time evolution of synthetic broad-band colours for a Salpeter IMF. Dashed lines represent models in which the TP-AGB contribution is not taken into account.

in a short time interval. Its early rise is due to the AGB phase transition starting at  $t \simeq 250$  Myr. The RGB phase transition takes place at  $t \simeq 500$  Myr, contributing to keep values high of  $(V-K)$ . The modest decrease in  $(V-K)$  at  $1 \text{ Gyr} \lesssim t \lesssim 4 \text{ Gyr}$  reflects the reduction of the TP-AGB contribution. The TP-AGB phase plays a major role in determining the IR colours at intermediate ages. This can be appreciated looking at models in which the TP-AGB contribution has been omitted (also shown in Fig. 10). The impact of the two phase transitions on optical colours is

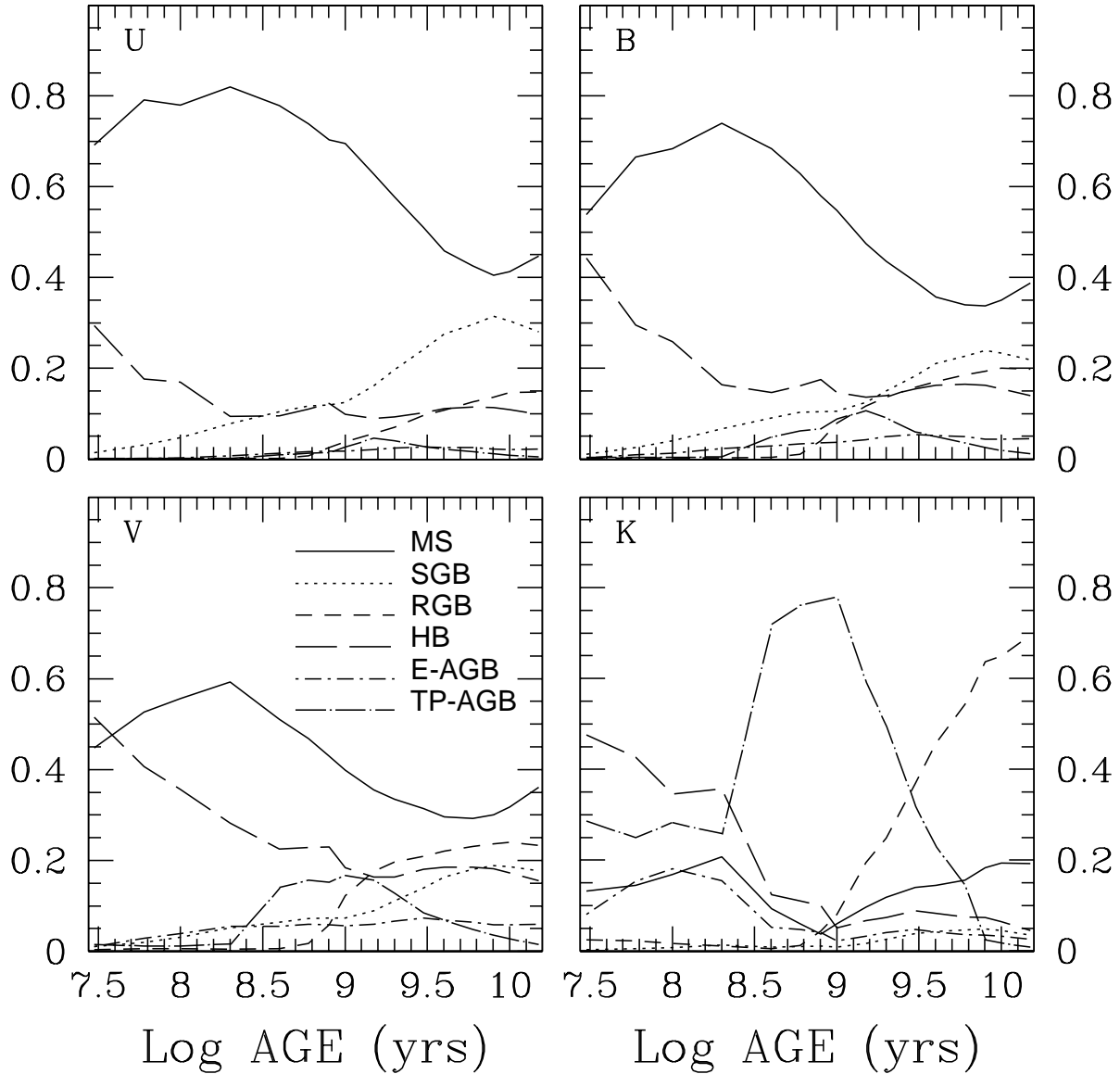


**Figure 11.** The evolutionary phase contributions to the total monochromatic luminosities,  $L_{ij}^{\lambda}/L_{i,T}^{\lambda}$ , as functions of the SSP age, for a Salpeter IMF.

much weaker as AGB and RGB stars radiate mostly in the near infrared.

The evolutionary behaviour of integrated colours can be easily understood by looking at the luminosity contributions of evolutionary stages,  $L_{ij}^{\lambda}/L_{i,T}^{\lambda}$ , shown in Fig. 11. The UVB emission mainly comes from MS stars at any age, except for  $t \lesssim 60$  Myr, when the major  $V$  contributors are He-burning supergiants of intermediate spectral type. The  $K$  band reveals the AGB phase transition at intermediate ages, when the TP-AGB contribution rises from  $\simeq 20$  per cent to  $\simeq 80$  per cent. The RGB phase transition is visible in all bands,

but particularly in  $K$ , where the RGB contribution dominates for  $t \geq 3$  Gyr. The IMF has no influence on integrated optical colours (Fig. 12), as the variations induced in  $U, B$  and  $V$  luminosities are nearly identical, leaving the corresponding colours unchanged. A small dependence is visible only in the infrared, at ages greater than  $\simeq 1$  Gyr, when a dwarf-dominated ( $x = 2.5$ ) SSP has colours redder than a Salpeter one, because of the contribution of low-mass stars. The Main Sequence contribution is the most sensitive to the IMF slope (see Fig. 13).

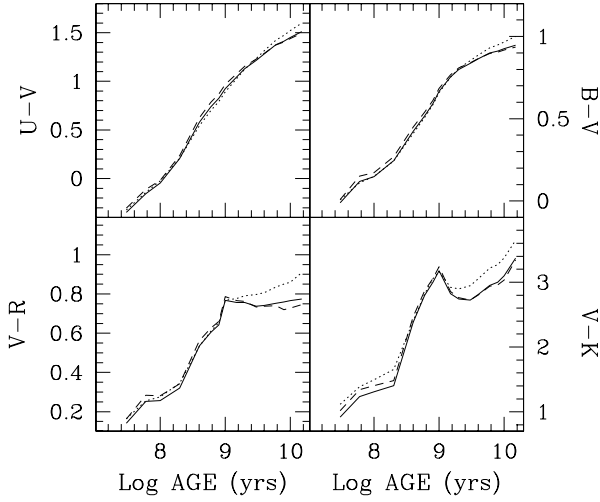


**Figure 12.** The influence of IMF on integrated broad-band colours: a Salpeter (solid line), a dwarf-dominated (dotted line) and a giant-dominated (dashed line) IMF.

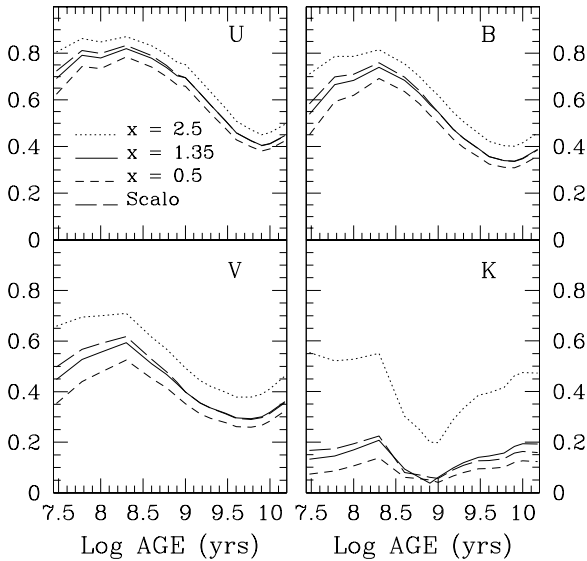


**Figure 13.** The dependence of MS luminosity contributions on the IMF slope, from a dwarf-dominated ( $x=2.5$ ) to a giant-dominated ( $x=0.5$ ) one;  $x=1.35$  is the classical Salpeter and Scalo refers to a three-slope IMF, defined in the caption of Fig. 2.

#### 4.2 The IMF scale factor

The size of a stellar population is directly connected to the scale factor  $A$  of the IMF. Thus it is useful to express  $A$  in terms of the integrated luminosity, which is also proportional to the size of a SSP and directly observable. To this aim, we solve eq. (4) for  $A$ , obtaining

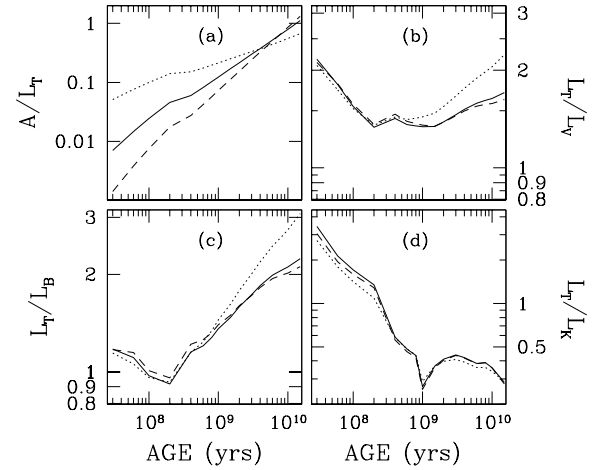


**Figure 14.** The relation between the scale factor  $A$  and the bolometric luminosity of a SSP,  $A/L_T^{\text{bol}}$  (panel a). Also shown are the bolometric correction factors  $B_c^\lambda$  (panels b,c,d), for three different choices of the IMF slope. Solid line refers to a Salpeter, dotted line to a dwarf-dominated ( $x = 2.5$ ) and dashed line to a giant-dominated ( $x = 0.5$ ) IMF.

$$A = B(t)L_T^{\text{bol}}(t)M_{\text{TO}}^{1+x} \left| \frac{dM_{\text{TO}}}{dt} \right|^{-1} \quad (11)$$

where  $B(t) = b(t)/L_T^{\text{bol}}(t)$  is the evolutionary flux per unit luminosity of the SSP (the ‘specific evolutionary flux’), a quantity nicely independent of the IMF slope (RB86). The total bolometric luminosity  $L_T^{\text{bol}}(t)$  is related to the total monochromatic ones  $L_T^\lambda(t)$ , through the bolometric correction factors  $B_c^\lambda(t)$

$$L_T^{\text{bol}}(t) = B_c^\lambda(t)L_T^\lambda(t). \quad (12)$$

$B_c^\lambda$  are functions of metallicity, IMF slope and age and are the direct product of synthetic SSP models. So, through eq. (11) and (12), we get  $A$  as a function of the luminosity in a certain band.

The ratio between the scale factor  $A$  and the bolometric luminosity, and the bolometric correction factors  $B_c^\lambda$  are shown in Fig. 14, all as functions of age and IMF slope. The  $L_T^{\text{bol}}/L_T^\lambda$  ratios are fairly independent of the IMF slope, as far as the IMF is not too steep for masses below  $\simeq 0.5 M_\odot$  (i.e.,  $1 + x \leq 2.5$ ). This is a consequence of the very narrow mass range producing most of the luminosity at nearly any SSP ages (see sec. 2). As an example, by adopting a Salpeter IMF, we obtain  $A \simeq 1.12 \cdot L_T^{\text{bol}} \simeq 2.5 \cdot L_T^{\text{B}}$  for a 15 Gyr SSP.

#### 4.3 The stellar mass-to-light ratio

At any age, an SSP is composed of ‘living’ stars and ‘dead-remnants’, according to the initial mass of stars. The stellar mass is given by the convolution of the present mass  $M(t)$  with the IMF. The present mass  $M(t)$  coincides with the initial mass ( $M(t) = M_{\text{in}}$ ) for  $M_{\text{in}} \leq M_{\text{TO}}(t)$  while  $M(t) = M_{\text{R}}$  (the remnant mass) for  $M_{\text{in}} > M_{\text{TO}}(t)$ . The kind of

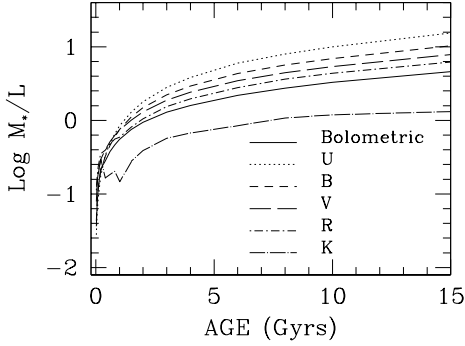


**Figure 15.** The evolution of stellar mass-to-light ratios for a Salpeter IMF.

remnant also depends on the initial stellar mass: here we adopt the following recipe (cf. Renzini & Ciotti 1993). For  $M_{\text{TO}}(t) \leq M_{\text{in}} < 8.5$ , the remnant is a white dwarf of mass  $M_{\text{R}} = 0.077 M_{\text{in}} + 0.48$ ; for  $8.5 \leq M_{\text{in}} < 40$ , stars leave a  $1.4 M_{\odot}$  neutron star; finally, stars with  $M_{\text{in}} \geq 40$  are assumed to leave massive black-holes of mass  $M_{\text{R}} = 0.5 M_{\text{in}}$ .

Fig. 15 shows the evolution of stellar mass-to-light ratios for the bolometric and  $U, B, V, R$  and  $K$  luminosities. The early time evolution of  $M_*/L$  is very fast, then, after an age of  $\simeq 5$  Gyr, it becomes mild. For example,  $M_*/L_{\text{T}}^{\text{bol}}$  increases of a factor of  $\simeq 15$  in the first 1 Gyr from the burst and only of a factor of  $\simeq 3$  from 5 Gyr to 15 Gyr. Fig. 16 shows the dependence of  $M_*/L$  on the IMF,  $M_{\text{inf}}$  being constant. At any age, the  $M_*/L$  ratios of a dwarf-dominated population ( $x = 2.5$ ) are much higher with respect to those of a population with a Salpeter or flatter IMF. For  $t \gtrsim 1$  Gyr a population with a top-heavy IMF ( $x = 0.5$ ) has  $M_*/L$  ratios larger than those of a Salpeter SSP, because of the larger number of heavy remnants.

The  $M_*/L$  trend is easily understood by looking at the evolution of the total stellar mass and its components (Fig. 17). The stellar mass of a dwarf-dominated SSP is mainly composed of living stars at nearly any age because of the long evolutionary time-scales of low mass stars. A giant-dominated ( $x=0.5$ ) SSP, on the contrary, has a larger amount of ‘remnants’ from massive stars.

We refer to a forthcoming paper for an analysis of the dependence of  $M_*/L$  on the SSP chemical composition.

## 5 COMPARISONS WITH STAR CLUSTERS

Synthetic broad-band colours and the luminosity contributions of evolutionary phases are now compared with the corresponding quantities for Globular Clusters, the natural counterparts of SSPs models. Population size effects limit

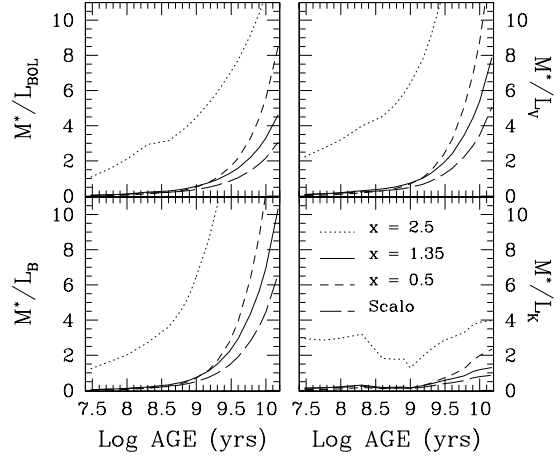


**Figure 16.** The dependence of stellar mass-to-light ratios on the IMF.

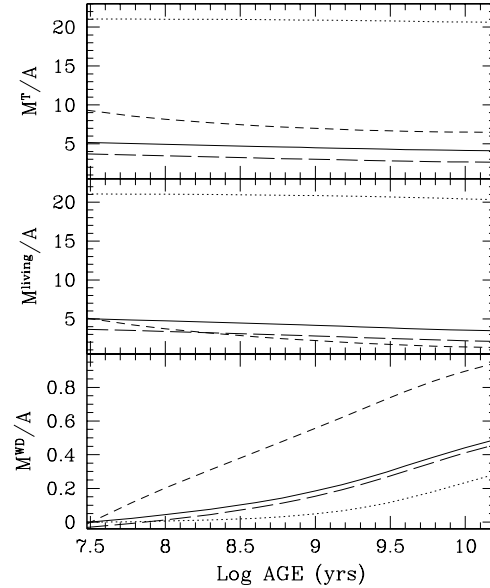


**Figure 17.** The evolution of the total stellar mass, the mass in living stars and the white dwarf component (from the top to the bottom). Solid line is for a Salpeter IMF, dotted line for a dwarf dominated IMF ( $x = 2.5$ ), dashed-line for a giant dominated IMF ( $x = 0.5$ ) and long-dashed line for a Scalo multislope IMF.

somewhat this comparison in the case of IR colours, as each cluster contains at most a few TP-AGB stars, hence stochastic fluctuations affect IR colours such as  $(V - K)$ .

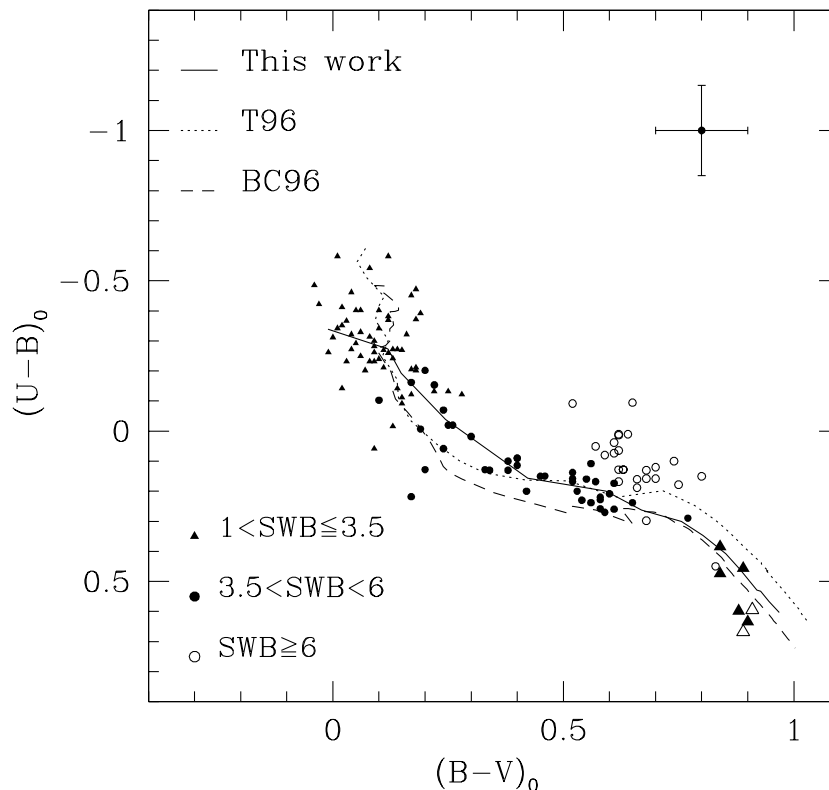


**Figure 18.**  $(U - B)$ - $(B - V)$  synthetic diagram, compared with LMC and Galactic globular cluster colours. LMC GCs data (from van den Bergh 1981) are represented according to the SWB classification scheme (see the text), as indicated by the labels at the bottom left. NGC 5927, NGC 6440, NGC 6624, Terzan 5, Pal 8 Galactic clusters (*full triangles*) and NGC 6528 and NGC 6553 Bulge clusters (*open triangles*) data are from Harris (1996). Reddening values have been taken from the authors and the typical error bar is indicated. T96 and BC96 solar models are also plotted.

### 5.1 Colour-colour diagrams

Fig. 18 shows our synthetic  $(U - B)$  versus  $(B - V)$  relation, compared with LMC GCs and Galactic clusters data. Observational  $(B - V)$  colours are corrected for reddening following the authors prescriptions; for Galactic clusters  $(U - B)$  colours, the relation  $E(U - B) = 0.8E(B - V)$  has been adopted. Tantalo et al. (1996; hereafter T96) and Bruzual & Charlot (1996, *private communication*; hereafter BC96) models are also plotted.

LMC clusters are grouped according to the SWB classification scheme and represented with different symbols (indicated by the labels in Fig. 18, 19 and 20). Types 1 to 3 correspond to young clusters ( $t \lesssim 120$  Myr, little fill triangles); types 3.5 to 5.5 to intermediate ones ( $250 \text{ Myr} \lesssim t \lesssim 2$  Gyr, fill dots) and types 6 to 7 to old ones ( $t \gtrsim 3$  Gyr, open circles).

The discrepancy between the models and LMC data for  $(B - V) \gtrsim 0.6$  is due to the increasing difference in the metal content. In fact, as already noticed, SWB types  $> 6$  are much more metal poor ( $Z \simeq 10^{-3} - 10^{-4}$ ) compared to earlier type clusters ( $Z \simeq 0.01$ ). This explains why they are bluer in spite of being older.

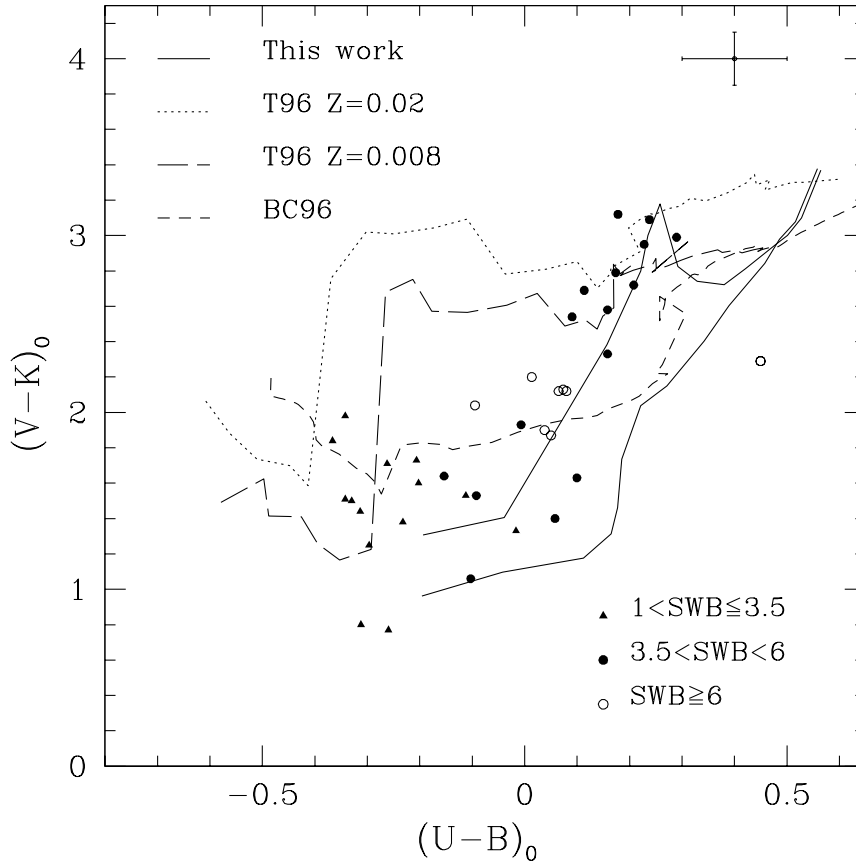
In the range  $(B - V) \lesssim 0.6$ , a good agreement is evident and the various models behave in much the same way. Galactic cluster colours are consistent with old ages, in agreement with the standard picture.

Fig. 19 shows  $(V - K)$  vs.  $(U - B)$  compared with a sample of LMC GCs with available infrared photometry (from Persson et al. 1983).

As it is well known, intermediate age LMC clusters exhibit a wide range of  $(V - K)$  values, from  $\sim 1$  to  $\sim 3.5$ . This is the result of the combined effect of AGB + RGB development, also visible in a  $(V - K)$  vs.  $(B - V)$  diagram (Fig. 20). The synthetic colours of our calibrated SSP model well agree with the observed ones, in this age range. T96 and BC96 models fail to reproduce the observed trend of IR colours at intermediate ages. Possible reasons will be discussed in the next paragraph.

### 5.2 Comparing different EPS

Analysing the discrepancies between different EPS models is not a simple job. Many factors contribute to produce different results, such as the stellar tracks used, the pho-



**Figure 19.**  $(V - K) - (U - B)$  two-colour diagram for the LMC GCs of Fig. 18 with available infrared photometry (from Persson et al. 1983); reddening values are taken from the authors and the typical error bar is indicated. As in Fig. 18, clusters are represented according to the SWB parameter (see labels at the bottom-right). T96 models for two different metal content and Bruzual & Charlot (1996, *private communication*) solar models are also plotted. The lowest solid line represents our SSP model in which the TP-AGB phase has been omitted.

tometric calibrations adopted to transform the theoretical Hertzsprung Russell diagram into observables and the synthesis method itself. In this section we limit ourselves to comment the discrepancy between synthetic  $(V - K)$  colours at intermediate ages, as shown in Fig. 19 and 20. The comparison is made with T96 and BC96.

Fig. 21 shows various synthetic broad-band colours as functions of age. The infrared indices of the three EPS models are quite different. The impact of AGB phase-transition at intermediate ages is visible only in our  $(V - K)$  model. T96 anticipate its occurrence, and their  $(V - K)$  shows a jump at  $t \sim 10^8$  yr. This is in contradiction with the observations. For example, the LMC cluster NGC 1866 ( $t \sim 10^8$  yr) does not have a developed AGB: according to FMB90, its AGB bolometric contribution is only the 6 per cent of the total.

T96 adopt the analytical prescriptions for the AGB phase as in Bressan, Chiosi & Fagotto 1994 (hereafter BCF94). These are based on the core mass-luminosity relation from Boothroyd & Sackmann (1988) and do not taken into account the results of Blöcker & Schönberner 1991 (see 3.2), as emphasized in BCF94 (see BCF94 for more details).

BC96 adopt a semi-empirical receipt (described in

Charlot & Bruzual 1991) to determine the position of TP-AGB stars on the theoretical CMD diagram. In their Fig. 4, the authors compare the predicted fractional luminosity contributions of the AGB with FMB90 data, as we do in Fig. 3, and a satisfactory agreement is evident. However, the integrated  $(V - K)$  of BC96 does not reach the high values observed in the intermediate-age LMC GCs. This is probably due to the energetic associated with C and M type stars (see Table 2). Furthermore, Charlot, Worthey & Bressan (1996) underline the lack of carbon star spectra in Bruzual & Charlot (1993) (and BC96) computations. The impact, on IR colours, of the amount of fuel burned by C or M type stars will be discussed in sec. 5.4.2.

At the end, it is clear that the major source of discrepancy between all models is the treatment of the AGB phase, as it controls the SSP infrared emission at intermediate ages (cf. Fig. 11).

On the opposite, the evolution of  $(U - B)$  and  $(B - V)$  is very similar for all sets of models. This arises from optical indices mainly depending on turn-off stars (cf. Fig. 11). The modest differences arise from the different input stellar tracks.

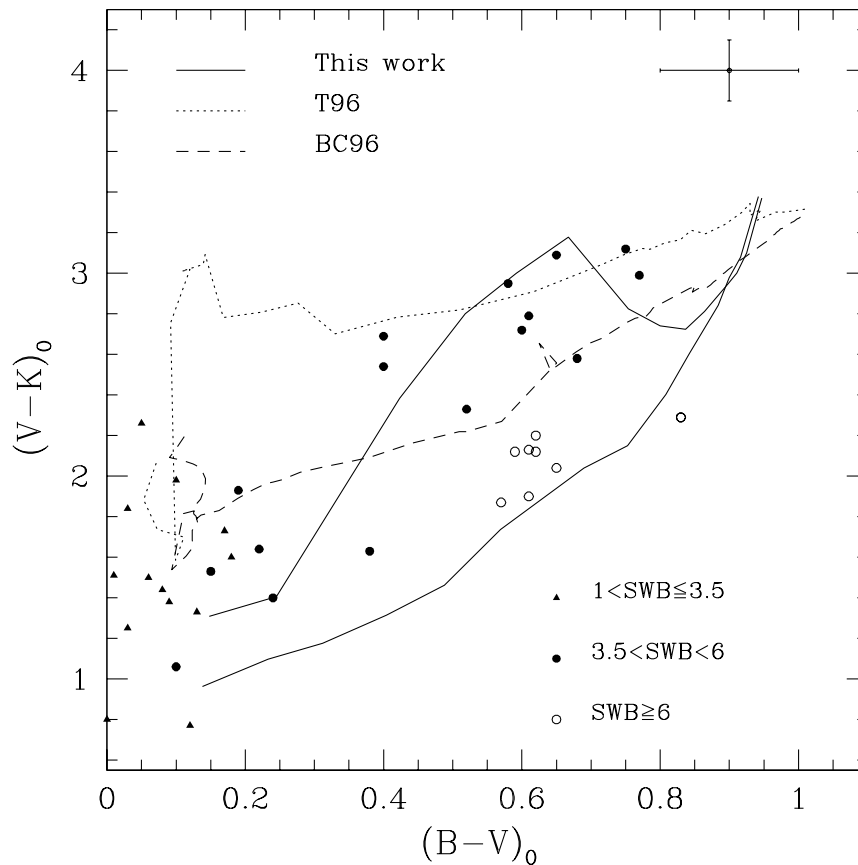


**Figure 20.**  $(V - K) - (B - V)$  two-colour diagram for the same LMC clusters and models as in Fig. 20.

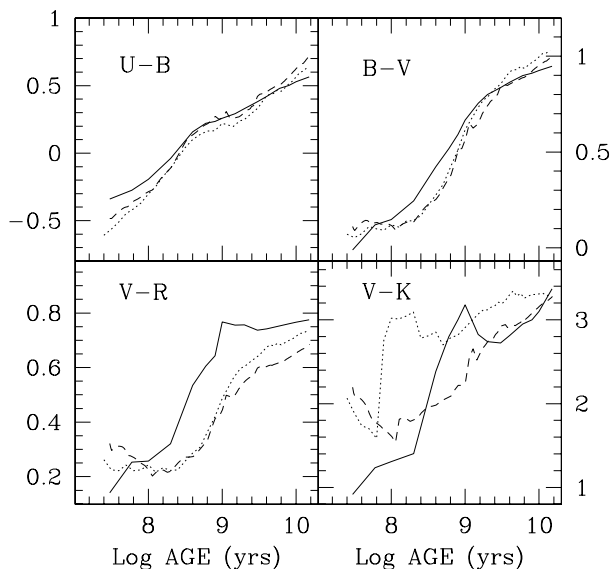


**Figure 21.** A comparison between different broad band colour models: this work (*solid line*); T96 (*dotted line*); BC96 (*dashed line*). All models assume a solar chemical composition, a Salpeter IMF, and a lower mass cutoff at  $0.1 M_{\odot}$ .

### 5.3 The luminosity contributions of evolutionary phases

A fundamental and global test for SSP models is the comparison of the synthetic luminosity contributions of the various evolutionary stages with the same quantities as measured in stellar clusters (cf. Renzini & Fusi Pecci 1988). We show the results of two tests of this kind.

The first test is performed on an intermediate age LMC GC sample (Ferraro et al. 1995; hereafter F95), selected with the aim of exploring the effect of AGB and RGB phase-transitions on integrated luminosities. The observed AGB and RGB contributions to the bolometric and  $K$  luminosity are compared with the synthetic quantities.

As emphasized by the authors, their cluster sample is rather limited (12 clusters in total) and the available star sample in each cluster is subjected to statistical fluctuations, especially in the case of AGB stars. AGB stars, whenever present, dominate the integrated cluster light, actually driving the IR magnitudes and colours, despite their small numbers. Anyway, the very short lifetimes involved ( $\sim 3.5$  Myr for the whole AGB, Iben & Renzini 1983) make highly fluctuating the AGB luminosity contributions from one cluster to another of nearly the same age. To limit this effect, clusters have further been grouped in age bins, following the procedure described in sec. 3.2. The LMC cluster NGC

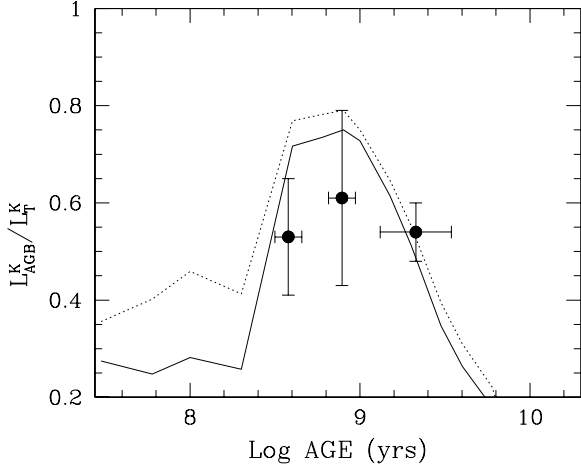


**Figure 22.** The AGB contribution to the total  $K$  luminosity compared with LMC GCs data from F95. The solid line represents the contribution of TP-AGB, while the dotted one refers to the whole AGB (i.e. E-AGB plus TP-AGB). Error bars indicate the r.m.s. (see the text).

1987 ( $s=35$ ) was not taken into account, because the AGB contribution is not properly defined in F95.

The cluster ages are derived from their  $s$ -parameter according to the relation  $\log t = 0.079s + 6.05$  (Elson & Fall 1988), as in F95. This relation is based on stellar evolutionary models by Vandenberg (1985), which adopt canonical convection (no overshooting). Our SSP models are based on a different set of stellar models (CCS92), which also adopt canonical convection. The two age-turnoff luminosity relations are very similar (to within  $\sim 10$  per cent) and therefore the Elson & Fall  $s$ -age relation is consistent with our SSP models. For an  $s$ -age relation from overshooting models see BCF94.

The results for the AGB phase are shown in Fig. 22. The solid line represents the synthetic TP-AGB contribution to the total  $K$ -light, and the dotted line refers to the whole AGB (that is, E-AGB plus TP-AGB). The error bars indicate the r.m.s.

The comparison shown in Fig. 22 suggests an agreement between the observed AGB phase transition and the synthetic luminosity contribution of the AGB phase, that, we recall, has been calibrated on the LMC GCs, as described in sec. 3.2.

Fig. 23 and 24 show the RGB contribution to the  $K$  and bolometric luminosities, compared with the same quantities from F95. Our model simulates the onset and early development of RGB phase transition very nicely.

For old ages ( $t \sim 15$  Gyr), the test is made with the  $\sim Z_{\odot}$  Bulge clusters NGC 6528 and NGC 6553, recently observed with HST (Ortolani et al. 1995).

The empirical contributions of evolutionary stages to the  $V$ -luminosity (Lanteri Cravet et al. 1997 and Lanteri Cravet, *private communication*) are compared with the cor-

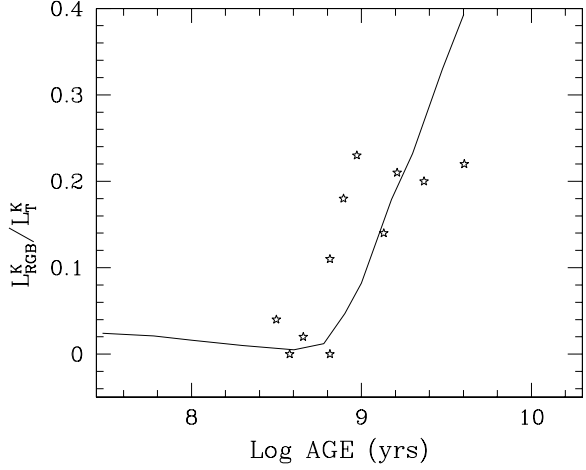


**Figure 23.** The RGB contribution to the total  $K$  luminosity compared to LMC GCs data from F95.

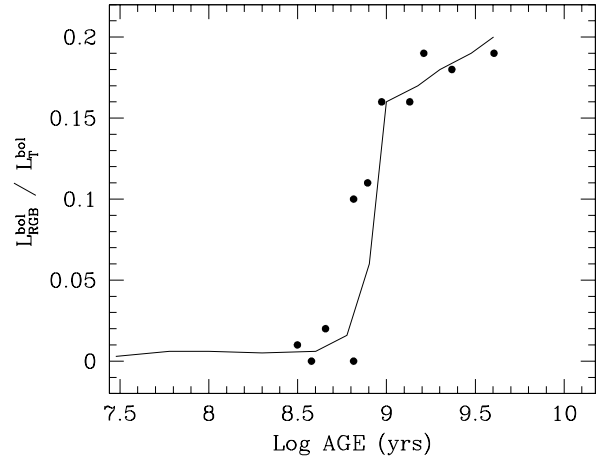


**Figure 24.** The RGB bolometric contribution compared to F95 data. The synthetic  $L_{\text{RGB}}^{\text{bol}}/L_{\text{T}}^{\text{bol}}$  takes into account that F95 sample is limited to 2.3 mag. fainter than the TIP of the RGB.

responding theoretical quantities in Table 5. To allow a more significant comparison, the synthetic MS  $V$ -luminosity has been truncated at the completeness limits of the samples ( $\sim 1.29$  mag. below the TO for NGC 6553, for which  $V_{\text{lim}}^{6553} = 21.5$ , Ortolani, *private communication*;  $\sim 2.95$  mag. below the TO, for NGC 6528, for which  $V_{\text{lim}}^{6528} = 23.6$ , Marconi, *private communication*). The theoretical contributions in Table 5 are fairly insensitive to the adopted IMF (see Table 6). In fact, down to the  $V_{\text{lim}}$  values quoted above, the stel-



**Table 5.** The contributions of evolutionary phases to the total  $V$ -luminosity (for a Salpeter IMF) compared with the observational data of the Bulge clusters NGC 6528 and NGC 6553 (Lanteri Cravet et al 1997 and lanteri Cravet *private communications*)

Phase $j$	NGC 6528	10 Gyr	15 Gyr	NGC 6553	10 Gyr	15 Gyr
MS + SGB	0.492±0.006	0.457	0.483	0.421 ±0.04	0.402	0.432
RGB	0.271 ±0.01	0.274	0.273	0.320 ±0.01	0.302	0.300
HB	0.154 ±0.02	0.181	0.163	0.180 ±0.01	0.199	0.179
AGB	0.083 ±0.02	0.087	0.081	0.08 ±0.01	0.096	0.089

**Table 6.** The IMF influence on evolutionary phase luminosity contributions of Table 6

Phase $j$	$\Delta V_{TO}^{\text{lim}} = 2.95$				$\Delta V_{TO}^{\text{lim}} = 1.29$			
	$x = 2.5$		$x = 0.5$		$x = 2.5$		$x = 0.5$	
	10 Gyr	15 Gyr	10 Gyr	15 Gyr	10 Gyr	15 Gyr	10 Gyr	15 Gyr
MS + SGB	0.476	0.502	0.444	0.471	0.410	0.441	0.397	0.425
RGB	0.265	0.263	0.281	0.280	0.298	0.295	0.305	0.303
HB	0.175	0.157	0.185	0.167	0.197	0.176	0.201	0.181
AGB	0.084	0.078	0.089	0.083	0.095	0.088	0.093	0.090

lar counts sample a small mass-range (for the 15 Gyr SSP we have:  $0.82 \lesssim M \leq 0.938$  for  $\Delta V_{TO}^{\text{lim}} = 1.29$ ,  $0.7 \lesssim M \leq 0.938$  for  $\Delta V_{TO}^{\text{lim}} = 2.95$ ). The agreement between predicted and observed contributions is quite satisfactory, and an old age ( $\simeq 15$  Gyr) seems to be favoured, in accordance with Ortolani et al. (1995) conclusions.

## 5.4 Two experiments

Thanks to the modular structure of the code it is possible to explore the impact of changing one or more ingredients and/or assumptions, on integrated photometric properties. We show here the results of two tests: the simulation of an ‘intermediate’ morphology for the Horizontal Branch at late ages, and the effect of a different contribution of  $M$  and carbon stars at intermediate ages.

### 5.4.1 Effect of a Blue HB

The location of the Helium-Burning (HB) stars of Globular Clusters on a HR diagram displays different morphologies, called ‘red-HB’ (RHB), ‘blue-HB’ (BHB) or ‘intermediate HB’ (IHB), depending on the observed extension towards blue. As well known, the HB morphology shows a correlation with cluster metallicity (the ‘first parameter’), but exceptions are so numerous that a ‘second parameter’ is required. The nature of this second parameter has not been firmly established, but commonly considered candidates include age and/or the cluster dynamical state (see Fusi Pecci et al. 1993). On average, metal-poor clusters have blue HB stars, while metal-rich ones show red HB. However, the presence of BHB stars in old, metal rich SSPs is theoretically plausible (see Greggio & Renzini 1990) and now observationally confirmed for some metal rich clusters in the galactic Bulge (Rich et al. 1997). In this section we explore the effect on integrated colours of adding BHB stars on the 15 Gyr SSP, while keeping constant the HB fuel consumption.

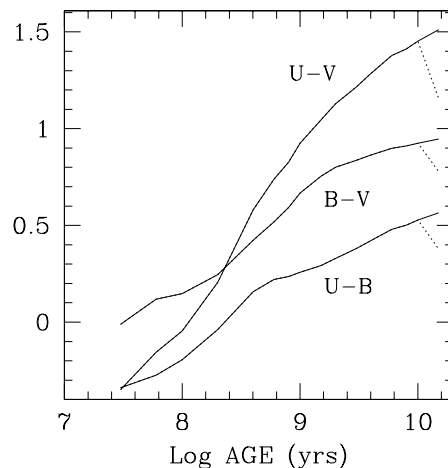


**Figure 25.** The effect on integrated colours of adding a BHB to the 15 Gyr SSP. Dotted lines are SSP models in which an intermediate HB morphology is simulated.

In this way, we simulate an IHB, as the red component is maintained. For this test we modify the  $(T_e, g)_{ij}$  matrix at  $t_i=15$  Gyr,  $j=HB$ , extending the temperature distribution to  $\log T_e \simeq 4$ ; a flat stellar distribution is assumed. The surface gravity for each effective temperature is derived assuming a constant luminosity.

The result is shown in Fig. 25. As expected, the  $(U-V)$  colour is the most influenced by the introduction of blue HB stars.

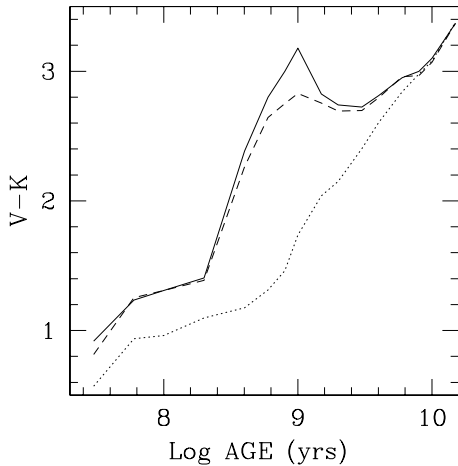


**Figure 26.** The influence of carbon stars populating the TP-AGB phase on integrated  $(V - K)$ . Solid and dotted lines are the models of Fig. 10 (including or not the TP-AGB contribution respectively); dashed line is a model in which the amount of TP-AGB fuel for C stars has been reduced by a factor of two.

#### 5.4.2 Varying the fraction of carbon stars

The initial metal content  $Z$  of a stellar population plays a key role in determining the production and the characteristics of carbon stars during the AGB phase (RV81). By reducing  $Z$ , the abundance of oxygen in the envelope is lower, thus a lower amount of carbon has to be dredge-up in order to achieve  $C/O > 1$  and create carbon stars. Therefore, a metal poor stellar population is expected to display much more carbon stars than a metal rich one of the same age. Passing from  $Z \sim 0.008$  (appropriate for LMC) to  $Z_{\odot}$ , the fraction of carbon stars is reduced by a factor of  $\sim 2$ . To estimate this effect on integrated colours, we have reduced by a factor of 2 the amount of fuel burned by C stars (see Table 2), assigning it to M stars.

Fig. 26 shows the result: the AGB phase-transition is still evident in the integrated  $(V - K)$  at intermediate ages, but the colour maximum value is reduced by  $\sim 0.4$  mag.

## 6 CONCLUSIONS

In this paper we have used the Fuel Consumption Theorem approach to compute evolutionary synthesis models (EPS) for Simple Stellar Populations (SSPs). The computational code has a modular structure, in which the main ingredients are kept as separate entries. This allows to investigate their impact on the results and to better assess the uncertainties. The TP-AGB contribution has been calibrated on LMC globular Clusters. A grid of SSP models, having a solar chemical composition and covering a wide age-range (30 Myr - 15 Gyr), has been constructed and submitted to several observational tests.

Synthetic broad-band colours, compared with LMC

GCs data, show a fair agreement. In particular, the observed rise in  $(V - K)$  colour at intermediate ages is well reproduced, as a consequence of the adopted calibration of the fuel consumption along the AGB phase. Comparing our results with others in the literature (Tantalo et al. 1996 and Bruzual & Charlot (1996; *private communication*), we show that only a correct calibration of the AGB energetics allows to match simultaneously the observed optical and IR properties of intermediate-age clusters.

A complete test of the luminosity contributions by the various synthetic evolutionary phases has been performed on the old Bulge clusters NGC 6553 and NGC 6528. The result is very satisfactory and an old age ( $t \simeq 15$  Gyr) for these clusters is favoured.

Having so tested the procedure, these models along with similar ones for other chemical compositions now being computed, will be used for a variety of astrophysical applications.

## ACKNOWLEDGMENTS

The author is indebted with Alvio Renzini and Laura Greggio for their guidance and for their critical reading of this paper. The author also gratefully acknowledges Luca Ciotti, Francesca Lanteri Cravet and Sergio Ortolani for many stimulating discussions. It is a pleasure to thank Gustavo Bruzual for kindly providing his SSP models in advance of publication and Oscar Straniero for his theoretical tracks in a computer readable form. It is also a pleasure to thank the European Southern Observatory and the Universität Sternwarte-München for their kind and generous hospitality during part of my research work. Finally, a special acknowledgement to the anonymous referee, whose helpful comments have greatly improved the presentation.

## REFERENCES

- Allen C. W., ‘Astrophysical Quantities’, Athlone Press, 1991
- Arimoto, N., Yoshii, Y., 1987, *A&A*, 173, 23
- Arribas, S., Martinez Roger, C., 1988, *A&A*, 206, 63
- Arribas, S., Martinez Roger, C., 1989, *A&A*, 215, 305
- Becker, S.A., 1981, *ApJS*, 45, 475
- Bessel M.S., Brett J. M., Scholz M., Wood P., R., 1989, *A&AS*, 77, 1
- Blöcker T., Schönberner D., 1991, *A&A*, 244, L43
- Boothroyd, A. L., Sackmann, I. J., 1988a, *ApJ*, 328, 632
- Bressan A., Chiosi C., Fagotto F., 1994, *ApJS*, 94, 63
- Bruzual G. A., 1983, *ApJ*, 273, 105
- Bruzual G. A., Charlot S., 1993, *ApJ*, 405, 538
- Bruzual G. A., Charlot S., 1996, *ApJ*, in preparation
- Buzzoni A., 1989, *ApJS*, 71, 817
- Castellani V., Chieffi A., Straniero O., 1992, *ApJS*, 78, 517
- Charlot S., Worthey G., and Bressan A., 1996, *ApJ*, 457, 625
- Charlot S., Bruzual, G., 1991, *ApJ*, 367, 126
- Chiosi C., Bertelli G., Bressan A., 1988, *A&A*, 196, 84
- Cohen J. G., 1982, *ApJ*, 258, 143
- Cohen J. G., Frogel J., A., Persson S., E., Elias J., H., 1981, 249, 481
- Elson R., A., W., Fall S., M., 1988, *AJ*, 96, 1383
- Ferraro F., Fusi Pecci F., Testa V., Greggio L., Corsi C.E., Buonanno R., Terndrup D.M., and Zinnecker H., 1995, *MNRAS*, 272, 391
- Frogel J. A., Mould J. R., Blanco V. M., 1990, *ApJ*, 352, 96

- Fusi Pecci F., Ferraro, F., Bellazzini, M., Djorgovsky, G., Piotto, G., & Buonanno, R., 1993, *AJ*, 105, 1145
- Greggio, L., Renzini, A., 1990, *ApJ*, 364, 35
- Guiderdoni, B., Rocca-Volmerange, B., 1987, *A&A*, 186, 1
- Harris W. E., Catalogue of Parameters For Milky Way Globular Clusters, McMaster University, revision 1 April 1996
- Iben, I., Jr., Renzini, A., 1983, *ARA&A*, 21, 271
- Johnson H., L., 1966, *ARA&A*, 4, 193
- Kurucz R., L., 1992, private communications
- Lanteri Cravet, F., Guarnieri, M. D., Renzini, A., Ortolani, S., 1997, in *Advances in Stellar Evolution*, ed. R. T. Rood & A. Renzini (Cambridge University Press), p. 59
- Ortolani, S., Renzini, A., Gilmozzi, R., Marconi, G., Barbuy, B., Bica, E., Rich, M., 1995a, *Nature*, 377, 701.
- Paczyński, B., 1970a, *Acta Astron*, 20, 47
- Paczyński, B., 1970b, *Acta Astron*, 20, 287
- Persson S. E., Aaronson M., Cohen J. G., Frogel J. A. and Mathews K., 1983, *ApJ*, 266, 105
- Renzini A., 1992, in B. Barbuy and A. Renzini, Dordrecht, Kluwer, 1992. IAU Symp. 149, The Stellar Populations of Galaxies, p. 325
- Renzini A., 1994, in “Galaxy Formation”, ed. J. Silk and N. Vittorio, (Amsterdam: North Holland), p. 303
- Renzini A., and Voli M., 1981, *A&A* 94, 175
- Renzini A., Buzzoni A., 1986 in *Spectral Evolution of Galaxies*, C. Chiosi and A. Renzini (eds.), Dordrecht, Reidel, p.195
- Renzini A., and Fusi Pecci F., 1988, *ARA&A*, 26, 199
- Renzini A., and Ciotti L., 1993, *ApJ* 416, L49
- Rich M. R. et al., 1997, astro-ph/9705039; to appear in *ApJL*
- Scalo, J. M., 1986, *Fund. Cosmic Phys.*, 11, 1
- Searle L., Wilkinson A., and Bagnuolo W.G., 1980, *ApJ* 239, 803
- Sweigart A. V., Gross, P.G., 1978, *ApJS*, 36, 405
- Sweigart A. V., Greggio L., Renzini A., 1989, *ApJS*, 69, 911
- Sweigart A. V., Greggio L., Renzini A., 1990, *ApJ*, 364, 527
- Tantalo R., Chiosi C., Bressan A., and Fagotto F., 1996, *A&A*, 311, 361
- Tinsley, B. M., 1980, *ApJ*, 241, 41
- van den Bergh S., 1981, *A&AS*, 46, 79
- VandenBerg D. A., Hartwick, F.D.A., Dawson P., Alexander, D. R., 1983, *ApJ*, 266, 747
- VandenBerg D. A., 1985, *ApJS*, 58, 711
- Westerlund B., E., Azzopardi, M., Breysacher, J., & Rebeirot, E., 1991, *A&AS*, 91, 425

## APPENDIX A: TABLES

The SSP models listed in the following tables refer to the TP-AGB fuel calibration described in Sec. 3.2.

**Table A1.** Integrated colours and stellar mass-to-light ratios as functions of age and IMF slope

AGE	$(U - V)$	$(U - B)$	$(B - V)$	$(V - R)$	$(V - K)$	$M^*/L_{bol}$	$M^*/L_U$	$M^*/L_B$	$M^*/L_V$	$M^*/L_R$	$M^*/L_K$
$x = 0.5$											
0.03	-0.305	-0.314	0.009	0.163	1.018	0.013	0.010	0.015	0.027	0.038	0.040
0.06	-0.113	-0.264	0.151	0.284	1.345	0.032	0.026	0.037	0.059	0.073	0.063
0.1	-0.019	-0.190	0.172	0.281	1.405	0.061	0.046	0.062	0.096	0.119	0.097
0.2	0.236	-0.033	0.269	0.342	1.481	0.134	0.111	0.128	0.183	0.216	0.173
0.4	0.626	0.177	0.449	0.562	2.468	0.199	0.253	0.243	0.292	0.281	0.111
0.6	0.786	0.245	0.540	0.626	2.868	0.300	0.419	0.377	0.417	0.378	0.139
0.8	0.871	0.259	0.611	0.660	3.056	0.400	0.595	0.528	0.548	0.481	0.168
1	0.968	0.283	0.685	0.786	3.237	0.506	0.815	0.708	0.685	0.536	0.128
1.5	1.078	0.312	0.767	0.766	2.857	0.774	1.369	1.158	1.040	0.829	0.276
2	1.154	0.344	0.809	0.762	2.760	1.048	2.046	1.679	1.450	1.160	0.422
3	1.229	0.388	0.840	0.734	2.723	1.609	3.520	2.774	2.327	1.911	0.701
4	1.290	0.425	0.865	0.738	2.803	2.150	5.141	3.919	3.216	2.638	0.899
6	1.375	0.480	0.896	0.741	2.940	3.275	8.773	6.356	5.068	4.137	1.250
8	1.404	0.499	0.905	0.720	2.960	4.416	12.323	8.773	6.935	5.774	1.716
10	1.440	0.523	0.917	0.728	3.035	5.557	16.122	11.221	8.780	7.251	1.983
15	1.495	0.559	0.936	0.746	3.343	8.496	26.606	17.959	13.785	11.205	2.347
$x = 1.35$											
0.03	-0.349	-0.339	-0.011	0.141	0.918	0.036	0.028	0.043	0.079	0.112	0.125
0.06	-0.155	-0.274	0.119	0.253	1.235	0.074	0.056	0.082	0.133	0.171	0.158
0.1	-0.046	-0.194	0.148	0.257	1.308	0.120	0.087	0.117	0.186	0.236	0.206
0.2	0.206	-0.039	0.245	0.321	1.405	0.220	0.171	0.201	0.292	0.351	0.297
0.4	0.580	0.157	0.423	0.535	2.384	0.279	0.330	0.322	0.397	0.391	0.163
0.6	0.739	0.221	0.518	0.605	2.800	0.377	0.493	0.454	0.512	0.474	0.182
0.8	0.827	0.235	0.592	0.643	3.000	0.465	0.653	0.593	0.625	0.560	0.202
1	0.924	0.258	0.667	0.767	3.178	0.552	0.843	0.750	0.740	0.588	0.146
1.5	1.045	0.292	0.754	0.756	2.824	0.753	1.289	1.111	1.009	0.812	0.277
2	1.129	0.329	0.800	0.757	2.741	0.941	1.797	1.496	1.303	1.047	0.386
3	1.216	0.380	0.837	0.737	2.723	1.289	2.810	2.232	1.879	1.539	0.566
4	1.285	0.421	0.864	0.742	2.812	1.591	3.836	2.940	2.410	1.965	0.669
6	1.378	0.479	0.899	0.753	2.950	2.187	5.995	4.347	3.460	2.791	0.840
8	1.413	0.501	0.911	0.760	3.000	2.753	7.969	5.658	4.447	3.641	1.069
10	1.452	0.528	0.925	0.766	3.100	3.295	10.012	6.948	5.389	4.364	1.181
15	1.512	0.565	0.947	0.775	3.370	4.616	15.446	10.332	7.867	6.227	1.306
$x = 2.5$											
0.03	-0.322	-0.329	0.007	0.165	1.116	1.076	0.806	1.231	2.226	3.087	2.946
0.06	-0.141	-0.252	0.111	0.256	1.387	1.596	1.187	1.688	2.773	3.535	2.859
0.1	-0.024	-0.173	0.149	0.276	1.497	2.095	1.521	2.011	3.190	3.994	2.971
0.2	0.209	-0.034	0.243	0.345	1.657	2.936	2.349	2.733	3.974	4.669	3.194
0.4	0.544	0.133	0.410	0.534	2.404	3.153	3.633	3.623	4.517	4.459	1.825
0.6	0.700	0.192	0.508	0.610	2.820	3.676	4.818	4.551	5.184	4.772	1.777
0.8	0.793	0.208	0.585	0.655	3.054	4.089	5.885	5.475	5.815	5.135	1.791
1	0.891	0.232	0.659	0.768	3.165	4.471	7.103	6.470	6.416	5.105	1.286
1.5	1.028	0.275	0.753	0.777	2.921	5.264	9.753	8.533	7.758	6.121	1.947
2	1.125	0.320	0.806	0.791	2.897	5.902	12.543	10.532	9.125	7.113	2.342
3	1.234	0.381	0.853	0.797	2.945	6.951	17.574	13.943	11.569	9.015	2.840
4	1.316	0.429	0.887	0.807	3.052	7.716	22.223	16.875	13.566	10.415	3.018
6	1.425	0.495	0.930	0.835	3.219	9.148	31.288	22.368	17.289	12.921	3.297
8	1.473	0.524	0.949	0.850	3.271	10.373	38.880	27.038	20.520	15.310	3.729
10	1.521	0.553	0.967	0.860	3.376	11.461	46.436	31.452	23.482	17.163	3.874
15	1.598	0.598	1.001	0.909	3.646	13.808	65.494	42.537	30.837	21.535	3.965

**Table A2.**  $A/L_T$  and the bolometric correction factors  $B_c^\lambda$ , as functions of age and IMF slope

AGE (Gyr)	$A/L_T$	$B_c^U$	$B_c^B$	$B_c^V$	$B_c^R$	$B_c^K$
$x = 0.5$						
0.03	0.001	0.778	1.171	2.114	2.938	3.062
0.06	0.004	0.798	1.147	1.816	2.256	1.946
0.1	0.008	0.752	1.010	1.569	1.955	1.591
0.2	0.017	0.826	0.959	1.363	1.606	1.289
0.4	0.027	1.271	1.217	1.464	1.409	0.557
0.6	0.042	1.397	1.256	1.390	1.260	0.463
0.8	0.057	1.488	1.321	1.368	1.203	0.421
1	0.073	1.609	1.398	1.354	1.060	0.254
1.5	0.113	1.769	1.497	1.345	1.072	0.358
2	0.155	1.952	1.602	1.384	1.107	0.403
3	0.241	2.187	1.723	1.446	1.187	0.436
4	0.325	2.391	1.823	1.496	1.227	0.419
6	0.500	2.679	1.941	1.548	1.263	0.382
8	0.678	2.790	1.987	1.570	1.307	0.389
10	0.855	2.901	2.019	1.580	1.305	0.357
15	1.314	3.132	2.114	1.623	1.319	0.276
$x = 1.35$						
0.03	0.007	0.765	1.177	2.164	3.066	3.434
0.06	0.015	0.763	1.107	1.805	2.308	2.141
0.1	0.024	0.722	0.973	1.546	1.969	1.714
0.2	0.046	0.786	0.918	1.333	1.601	1.351
0.4	0.060	1.180	1.151	1.419	1.399	0.584
0.6	0.082	1.309	1.204	1.359	1.256	0.482
0.8	0.102	1.406	1.277	1.346	1.202	0.436
1	0.123	1.529	1.360	1.339	1.067	0.265
1.5	0.170	1.712	1.474	1.340	1.078	0.368
2	0.215	1.910	1.590	1.385	1.113	0.410
3	0.299	2.179	1.731	1.457	1.193	0.439
4	0.373	2.410	1.846	1.515	1.235	0.420
6	0.520	2.741	1.988	1.581	1.276	0.383
8	0.659	2.895	2.056	1.616	1.323	0.389
10	0.793	3.039	2.109	1.636	1.325	0.358
15	1.120	3.345	2.238	1.704	1.349	0.283
$x = 2.5$						
0.03	0.051	0.750	1.144	2.069	2.869	2.738
0.06	0.076	0.744	1.058	1.737	2.214	1.791
0.1	0.100	0.726	0.960	1.523	1.907	1.418
0.2	0.140	0.800	0.931	1.354	1.590	1.088
0.4	0.150	1.152	1.149	1.433	1.414	0.579
0.6	0.176	1.310	1.238	1.410	1.298	0.483
0.8	0.196	1.439	1.339	1.422	1.256	0.438
1	0.214	1.589	1.447	1.435	1.142	0.288
1.5	0.252	1.853	1.621	1.474	1.163	0.370
2	0.283	2.125	1.785	1.546	1.205	0.397
3	0.334	2.528	2.006	1.664	1.297	0.409
4	0.372	2.880	2.187	1.758	1.350	0.391
6	0.442	3.420	2.445	1.890	1.412	0.360
8	0.502	3.748	2.607	1.978	1.476	0.360
10	0.555	4.052	2.744	2.049	1.498	0.338
15	0.669	4.743	3.080	2.233	1.559	0.287